MICROMETEORITE CRATERS ON LUNAR ROCK SURFACES

F. Hörz

The Lunar Science Institute

Houston, Texas

J. B. Hartung

NASA - Manned Space Craft Center

Houston, Texas

D. E. Gault

NASA - Ames Research Center

Moffett Field, California

•Lunar Science Institute Contribution No. 09

ABSTRACT:

Detailed optical stereomicroscope study of seven lunar rocks (12006, 12017, 12021, 12038, 12047, 12051, 12073) has been made. Common microcraters on crystalline rock surfaces consist of a central glass-lined "pit" surrounded by a crush-zone or "halo" of micro-fractured crystalline material both of which lie within a "spall" area produced by the impact event. Crater diameters measured range from smaller than .1 mm up to several millimeters. The ratios of halo diameter to pit diameter and spall diameter to pit diameter average 2.3 and 4.5 respectively. The glass lining of most pits is melted host rock. Based on laboratory cratering experiments which yield glass-lined pits, at least 95% of the microcraters observed are interpreted as the impacts of primary cosmic particles moving at relative velocities greater than 10 km/sec. A sharp demarcation line between cratered and completely uncratered rock surfaces indicates that parts of some rocks were buried in the lunar soil. The presence of "ropy splashes" and "welded" dust near the soil line of the rock is evidence of secondary impacts related to primary impacts occurring in the soil near the rock. Microcratering on the millimeter scale is the dominant process causing erosion of rock surfaces exposed to the lunar environment.

Microcrater populations on glass-covered rock surfaces are not "equilibrium" populations, otherwise the cratering process would have removed the glass coatings entirely. The size distribution of these microcraters corresponds with the interplanetary particle mass distribution and indicates that on the log cumulative flux versus log particle mass curve a negative slope of greater than one exists down to masses in the 10^{-7} - 10^{-8} gm range. Using currently accepted particle flux data based on satellite-borne experiments a minimum exposure time for the glass surface on rock 12073 is 10^{3} years.

The populations of millimeter-sized microcraters on the most cratered surfaces of all rocks examined are "equilibrium" populations. The minimum time required to achieve the state of equilibrium on the rocks studied is about 10^{5} years.

The mean survival times of the seven rocks are calculated to $.5\text{-}3.5\text{x}10^{6}$ years using empirical data on rock destruction by meteroid impact. A similar approach is used to derive a minimum erosion rate of .2 - .4 mm in 10^{6} years. However all these data are heavily dependent on the interplanetary particle flux applied and thus highly tentative.

OUTLINE

INTRODUCTION

Investigations of natural and experimental impact craters have become an increasingly important tool for the interpretation of planetary surface processes, especially those on the Moon. Over geologic time the lunar surface has been repeatedly impacted. Lunar impact craters range in size over at least eleven orders of magnitude, thus reflecting a wide variation in mass and/or velocity of cosmic bodies (Shoemaker et al., 1969, Shoemaker et al., 1970, Gault et al., 1968, and many others). A continuous range of craters down to cm sizes could be observed in the Orbiter and Surveyor photographic series, the lower size limit always being the resolution of the optical system employed.

With the return of actual lunar surface material during Apollo 11 and 12 (PET-Report 1969a and 1969b) it was learned, that most of the rock surfaces are heavily pitted by craters in the .1 to 3 mm range. McKay et al. (1970), Carter and McGregor (1970) and Neukum et al. (1970) reported craters a few microns in diameter on individual grains of lunar soil using scanning electron microscope techniques.

It is the object of this report to summarize detailed stereo-microscopic studies of nearly 5000 craters in the .1 to 3 mm size range observed on 7 whole rocks returned during Apollo 12. It is intended to evaluate the conditions of formation of these craters and to relate the observed crater populations to the flux of primary cosmic particles. Knowledge of cosmic particle flux contributes to our understanding of cosmic erosion, survival times of rocks on the lunar surface and related problems.

EXPERIMENTAL TECHNIQUES:

Whole rock surfaces were studied using a stereomicroscope. Each rock was mounted in a gimballed holder which could be moved horizontally, thus providing a maximum of surface area for observation with a minimum of handling. The rock holder and microscope were contained in a plastic bag filled with dry nitrogen. Eyepieces and photographic optics penetrated the plastic bag. The microscope and holder were operated through gloved ports in the bag.

The position of each field of view was indicated on photographs of the rocks taken at the NASA-MSC Lunar Receiving Laboratory. For each field of view the total number of craters was recorded. Counts obtained by different individuals on the same surfaces could deviate by up to 40% for craters in the .4 to 1 mm classes though in general the results agreed to better than 20%; deviations of individual observers were within 10% for craters larger than 1.2 mm.

For each field of view estimates were made of the surface areas occupied by cracks, large vugs, dust covered patches, steep surface slopes, etc. in order to obtain the total surface area potentially suitable to display microcraters. Fields of view containing large cracks etc. were omitted from the statistical evaluations.

Only Apollo 12 rocks were investigated (Figures 1 and 2). They included both fine grained (12006, 12038, 12047, 12051) and coarse grained 12017, 12021) crystalline rocks. Rock 12073 was a fine grained breccia similar to those returned during Apollo 11 mission. Rocks 12017 and 12073 had surface areas which were partially coated with

glass. Thus the rock surfaces varied widely in grain-size and in their suitability to quantitatively detect the microcrater populations. The ease of recognition of microcraters decreased from glass surfaces over breccias and fine grained to coarse grained rocks. Craters of sizes smaller than 1 mm become increasingly more difficult to be recorded quantitatively. Therefore the lower end of craters recorded was arbitrarily set at .4 mm. Actually "pit" diameters (see below) were recorded, i.e. the cut off was set at .1 mm "pit" diameter.

MICROSCOPIC INVESTIGATIONS

CRATERS ON CRYSTALLINE SURFACES:

The morphology of the craters observed are more complex than previously described (PET report 1969a and 1969b). The morphologic elements used to describe the shapes of microcraters are schematically defined in Figure 3 and illustrated in Figure 4.

Central Pit:

A central, glass lined depression termed "pit" is the most characteristic element of lunar microcraters. Only a few pits are perfectly circular; most of them have irregular, jagged outlines (Figure 5). On fine grained crystalline rocks the pits are in general more circular than on coarse grained surfaces.

Non-circularity of the pit is probably caused by different mechanical properties of the component minerals; shock impedance, strength anisotropies etc. exert control over the propagating shock front and thus over the melting and excavation process. This was

particularily well illustrated by a few oval shaped pits which were formed in plagioclase bordered by pyroxene laths. Oval shaped craters had a maximum ratio of long/short axis of 1.5. The pit bottoms are in general more centrosymmetric than the upper parts of the pit walls.

Fresh pits show lips of shock melted glass. These lips are in general highly irregular in circularity and surface relief. Some have tear drop shaped promontories; some lips had collapsed while still in a fluid state and sagged onto the rock. Occasionally the glass had flowed on the surrounding target without forming a distinct lip (Figure 6). In rare cases glass droplets outside the pit can be associated with this particular impact event.

Most glass linings display under high magnification a variety of colors. These glass colors correspond qualitatively to the mineral phases with which they are in contact, i.e. feldspar results in clear glass, pyroxene in dark to honey brown shades, olivine in yellow-green colors and ilmenite produces a pitch black glass. Roughly 30% of 225 randomly selected pits on rock 12038 have distributions of glass colors which proportionally correspond to the mineral phases present. About 60% of the pit glasses correspond to the target minerals, although they do not precisely match the target proportions. About 10% of the glass linings display colors which are either grossly out of proportion with respect to target minerals or have no relation at all to them. The latter ones are exclusively of darker shades, perhaps suggesting the admixture of iron bearing projectile material. Pits of this category are e.g.

pits confined to single plagioclase crystals and yet display black glass linings only. These studies of distribution of colors in glass linings are highly qualitative and can by no means replace chemical analysis. However it seems that the vast majority of pit glasses may be derived in situ from the target minerals due to shock fusion.

The surface of the pit linings shows a wide variety of textures and surface reliefs, ranging from completely smooth to ropy and highly irregular, hummocky surfaces (Figure 6). The degree of surface relief in general seems to be somewhat related to the glass composition, i.e. to the glass color, though exceptions to this rule are not infrequent. The clear feldspar glasses seem to be mostly very smooth; pits lined with 100% clear glass are without exceptions always smooth. In multicolored pits the clear glasses are mostly the smoother ones as compared to brown and black glasses. Only in a few cases the glass flowed down the pit wall as evidenced by tear drop shaped flow fronts. Mostly the surface relief cannot be explained by flow alone.

Halo Area:

All glass lined pits were surrounded by a concentric zone of highly fractured target materials termed "halo" (see Figures 3, 4, and 5). This relatively high albedo material aids considerably in the recognition of pit craters. A gradual transition between the highly fractured materials and unaffected rock was observed. Halos are particularily evident in feldspars. Microfractured pyroxenes and olivines are of light brown color; ilmenite retains its black color even in a highly fractured state.

Though the vertical extension of halos could rarely be observed, it is reasonable to consider this microfractured material to occupy a roughly hemispherical volume surrounding the pit (Engelhardt et al., 1970). On densely cratered surfaces halo material in between closely spaced impact pits forms a continuous microfractured surface. This surface is noticeably lighter in color and gives the rock a shocked appearance. However the depth of the shocked material is generally less than 1 mm.

Spall Zones:

Pits on crystalline surfaces associated with easily observed spall areas are mostly fresh and commonly have well preserved lips. About 20% of the pits studied are surrounded by observable spall plates. Spall zones are especially pronounced where the surface relief of the rock was such that small promontories were partially or completely removed or where free surfaces of cracks, vugs and other depressions facilitated the removal of material.

The existence of a spall zone could never be excluded in all events observed. All halo areas are concentrically surrounded by a zone exposing fresh appearing crystalline rocks. This was especially well illustrated in rock 12006, some surfaces of which are thoroughly covered by a non-transparent, dusty coating (see later on). The micrometeorites penetrated the dust coating, forming a pit, halo material and a somewhat larger, concentric zone of well exposed, fresh substrate, easily visible around <u>all</u> craters on this rock.

The geometries of fresh lunar microcraters are compatible in all respects with craters produced in the laboratory (Moore et al., 1965, Gault, 1969, Hörz, 1968, Vedder, 1970). Hence it is reasonable to assume that all of the pits observed were originally surrounded by spall plates. The lunar microcraters are by no means as unique in geometry as originally proposed (P.E.T., 1969).

Deviations from circular spall outlines are common in coarse grained rocks. The degree of circularity increases with decreasing grain size. The most dominating factor for circularity however is the degree of surface relief at the target site. Promontories, valleys etc. control the spallation effectively. Therefore the most common evidence for spallation is a fraction of a concentric segment only, rather than a perfectly circular depression.

No statistical measurements of the spall area's precise three dimensional shape have been carried out. However, the spall plate geometries vary considerably in cross-section as illustrated in a highly idealized sketch (Figure 7). All transitions between these geometries are possible and have been observed on all rock surfaces. No cratering experiments are available at present to relate the various spall plate geometries with possibly different formation conditions.

Stylus Pits:

One of the most striking feature for some pits is that they are morphologically higher than the surrounding halo area (P.E.T., 1970). Within the excavated crater zone they form a positive topographic feature. Commonly the pit sits on a pedestal or stylus; these features were

termed "stylus pits" (Fi 8). y idealized sketch (Figure 9) illustrates the varie n thei es. All transitions between the shapes indicated oc

At first glance t pe stals to be due to erosion processes after crate ma The all scarcity of such stylus pits howe s to ate not all of the craters are subject to th ocess. addit. "stylus pits" were observed which displayed we. eserve ater and pronounced spall zones thus indicating a g e ent n two ances small glass droplets, undoubtedly origi ng com glass , were visible in the excavated zone ar d t . The bservations suggest that the removal of m cial lea to the mation of the stylus is a primary effect cur in ng the r forming event. This conclusion is orted observat. hat large stylus pits are formed pr nantl previously s ed surfaces where mass removal wa litate re-existing ofractures. Specific formation tions f ylus pits are nown at present. No laboratory analogues ailable.

Crater Dimensions:

The parameters use describe the geometries of microcraters are pit- halo- and spall diameter which were measured against a calibrated eyepiece. Summaries of the pit diameters observed are illustrated in Figure 10. The number of pits indicated for the smallest size class is not necessarily representative because smaller

pits become increasingly difficult to recognize. Pits of much larger diameters than those observed cannot be expected on rocks of the sizes investigated because such crater-producing events would completely rupture the rock (Gault and Wedekind, 1969).

The measurements for halo- and spall-diameters were only carried out until reliable statistics for ratios of pit/spall diameters and pit/halo diameters were obtained. The results are plotted in Figure 11. Variations in D_H/D_P and D_S/D_P are probably caused by relative abundances of target minerals, different impact velocities, the intensity of fracturing of the rock surface caused by previous cratering and measuring inaccuracies, especially for the smaller crater sizes. Average ratios are 4.5 and 2.2 for spall/pit and halo/pit diameters respectively.

CRATERS ON BRECCIA SURFACES:

The crater morphologies observed on rock 12073 - the only fine-grained breccia returned during Apollo 12 - are almost identical to those observed on the crystalline rocks. The only deviations are subtle in character owing to a more fine grained target. The pits are more circular. Halos are less prominent due to the lack of large feldspar crystals. Spall zones are well developed and more circular if not perturbed by the rock's surface relief. The extremely fine-grained and relatively homogeneous breccia matrix displays pit linings of uniform dark brown colors only. The pit diameters measured on rock 12073 are illustrated in Figure 11. Ratios of spall to pit diameters also cluster around values of 4.5.

CRATERS ON GLASS SURFACES:

Rocks 12073 and 12017 display surfaces partially covered with a thin, coherent coating of glass. Small craters in the .1 to .4 mm size class are frequent on these glasses (Figure 13). The craters have a central pit, a pronounced spall zone and a less prominent halo zone. In addition they have a distinct rim surrounding the pit which was never observed on crystalline rocks and breccias. The glass coatings display by far the most centrosymmetric craters of all surfaces investigated. Ratios of pit/spall cluster about a value of 4.3. Size frequency relations of spall diameters are illustrated in Figure 14. (Owing to their small size, measurements of the pit diameters seemed to be too inaccurate for the optical system employed). The crater geometries observed are similar to even smaller craters reported from lunar fines (McKay et al., 1970, Carter and MacGregor, 1970, Neukum et al., 1970) and to those produced by microparticle accelerators in laboratory studies (Vedder, 1970).

Projectiles of sufficient energy were able to penetrate the thin (.05 - .5 mm) glass coating as illustrated in Figure 15. Such events produced a glass-lined pit in the substrate and caused a large amount of glass coating to spall. Spall zones in such a target configuration are particularily evident. Pit/spall diameter ratios of 1:6 and larger were commonly observed.

PITLESS CRATERS:

All phenomena described so far were characterized by central glass-lined pits. The presence of shock-melted glass indicates high impact energies per projectile mass unit. These features account for 80 - 90% of all cratering phenomena observed. Another 10% consists of depressions (on all 3 types of rock surfaces) which are not associated with any fusion products and therefore are considered to be due to low velocity impacts (McKay, 1970).

As indicated in Figure 16, they can be of cone or round bottom shape. About 90% of these features are associated with various amounts of halo material with types 16b and 16c being the most abundant ones. Only about 10% are not associated with intense microfracturing. Features of type 16d could be bona fide high velocity craters with the central pit removed. Such an interpretation is especially plausible for craters displaying spall zones which are in general very rare for all other low velocity features.

Occasionally flat halo areas were observed, completely unrelated to any depression. They also can be due to low speed collisions, but it is more likely that they are the remainders of a deeply eroded, genuine pit crater.

FEATURES RELATED TO METEORITE IMPACT:

LARGE GLASS COATINGS:

Rocks 12073 and 12017 display large surface areas ($\approx$5 cm^2 and 7 cm^2) which were partially coated by a veneer of dark brown glass varying in thickness from .05 to .5 mm (P.E.T., 1970). Both coatings are

characterized by an extremely smooth surface (Figure 17, see also Figure 1). The overall relief of these glass surfaces is strongly controlled by the underlying rock. The contacts of the glass coatings with the substrate are characterized by either a gradual pinching out of the glass which can be associated with fine glass droplets or by relatively thick (.2 - .5 mm) "flow fronts". The melt also flowed around edges and corners of the rock. Surface tension and viscosity must have been such that the glass could contract leaving "fensters" through which the substrate is visible. Well-defined schlieren were observed on glass 12017 (Figure 17 and 15).

Rocks 12017 was broken off on one side. The contact between glass and crystalline substrate could be studied in cross section. All along the exposed contact the crystalline material was highly microfractured, i.e. identical to halo material (Figure 18). This material was unequivocally associated with the deposition of the glass.

The thinness in comparison with the lateral distribution, the smoothness of the coating's surface and the gradual pinching out indicate a highly fluid melt. The abundance of schlieren suggests very strongly shock compression as the heat source for the fusion process. In addition, the glass must have been deposited on the rock at velocities high enough to shock fracture the substrate. No observations are available to be able to distinguish between whether the collision with the rock occurred in flight or while the rock

was resting on the lunar surface. The coatings could also be part of the shock melted material from the walls or bottom of larger scale impacts because the astronauts reported glass coated rocks sitting in or around meter sized craters (PET Report 1969a and 1969b).

Rock 12017 displays a "second generation" glass of somewhat darker color on top of the big glass coating (Figure 17). Such glasses are found as teardrop-shaped or extremely narrow, elongated splashes. This indicates again a deposition in a highly fluid state. Mass and/or velocity during deposition of the splashes must have been such that they did not fracture the first generation glass. On close examination even these small splashes display schlieren. No hints about the time lapse between first and second generation glasses could be established.

On the basis of closeup stereophotos taken directly on the lunar surface, Gold (1969, 1970) proposed as a possible formation mechanism for some glass coatings on the lunar surface the direct fusion of rocks due to spasmodic, extremely energetic, radiative heat from the sun. A variety of arguments against such a hypothesis were brought forward by Green (1970), Dietz and Vergano, (1970) and Greenwood and Heiken (1970). Greenwood and Heiken suggested shock compression as the melt-producing process. The relative abundance of schlieren is typical for shock-produced glasses. In addition the glasses must have coated the rock with some relative velocity, the evidence for which is the shocked substrate and teardrop-shaped, second generation "splashes" on rock 12017. Although our evidence

is based on observations on two rocks only, we feel in accordance with Greenwood and Heiken, that shock compression as a glass forming process offers the most reasonable explanation of the glass coatings observed on the lunar surface.

ROPY GLASS SPLASHES:

Some glass patches differ from the above mentioned glass coatings not only by highly irregular outlines, but especially in size. They are commonly .3 to 10 mm across. The surfaces of these patches are hummocky and ropy and they may have a dusty appearance. These patches are termed "ropy glass splashes" (Figure 19).

All ropy glass splashes are underlain by halo material and some are surrounded by spall plates. The halo zone is characteristically .1 to .2 mm wide regardless of the size of the splash. The color of ropy glass is dark brown to black and is unrelated to target composition; no vari-colored glasses were observed.

Ropy glass splashes may be mistaken for the bottom segment of an eroded glass lined pit. The relatively narrow halo zone, the extremely rough, dusty surface and a color unrelated to the host rock allow however their distinction. Furthermore the ropy glass splashes represent an "addition" of material to the rock while pit craters are characterized by removal of material. Rocks 12021 and 12038 give some clue to the origin of ropy glass splashes. Although ropy splashes principally do occur on all cratered rock surfaces, they are concentrated in areas where other evidence points to a contact with the surface of the lunar soil (see below). Thus we interpret

these ropy splashes as ejecta of microcratering events happening in the lunar soil next to the rock. They probably are materials thrown against the rock as a mixture of shock-melted glass and unshocked lunar soil, giving rise to the dusty, hummocky surface and to the shock effects in the target minerals.

WELDED DUST:

Intermittent patches (up to .5 cm^2) of non-transparent, glassy material of rough, hummocky relief and dusty appearance were observed. These patches are much thinner ($\approx$20-50 μ) than ropy glass splashes. However, the underlying rocks display no halo material; spall zones were not observed. Welded dust seems also to be concentrated around the "soil line".

It is concluded that these intermittant patches are similar to ropy splashes in origin (Figure 20). They are just a "thinner" version of ropy splashes containing proportionately more dust. Their masses and/or velocities were not sufficient to shock fracture the crystalline substrate.

THIN FILM COATING:

In contrast to the non-transparent "welded" dust, patches of extremely thin (probably less than 10 μ) glass coatings were observed which were transparent. They are similar in occurrence and size to welded dust. Coated areas are darker than freshly broken crystalline surfaces. They lack any dusty surface appearance. They possibly represent an extremely thin version of "welded dust" containing much less unshocked material. More likely they are however

condensed silicate vapors from micro impacts in the soil or on the rock itself. This explanation is suggested by the concentric arrangement of thin film coating outside the spall zone on one extremely large pit crater on rock 12051.

FROSTING:

Some crystalline rock surfaces appear to possess dull reflectivity termed "frosting". Frosting is removal of material on a very minute scale leaving single crystal faces without vitreous luster (Figure 21). If present, it is common to the entire mineral assemblage of some specific rock surfaces. Such surfaces were observed on rocks 12021, 12038 and 12051. The surfaces on rocks 12038 and 12051 display absolutely no craters; the surface of rock 12021 was by far the least cratered surface observed.

Frosting was practically never observed on cratered crystalline surfaces as well as on glass coatings; the fine grain size of breccias prevent its identification. About 30% - 50% of single idiomorphic vug minerals however display frosted crystal faces. Frosting is virtually absent on glass linings of pits. A possible explanation for frosting will be given below.

MICROPARTICLE IMPACT EXPERIMENTS

Some photographs of microparticle impact craters produced by J. F. Vedder, NASA-Ames Research Center are shown in Figure 22. The projectiles were launched with an electrostatic microparticle accelerator. Projectile and target materials, projectile mass and impact velocities closely approach lunar environmental conditions.

These preliminary data indicate that genuine glass-lined pits are formed at impact velocities exceeding 10 km/sec for Al-projectiles. However even at these velocities the energy per projectile mass unit seems not sufficient to cause a complete removal of the spall plates. Some additional energy is necessary to cause the spall plates to fly away. Consequently we conclude that 10 km/sec is a conservative estimate of the minimum impact velocity to produce lunar microcraters of the kind observed.

INTERPRETATION AND DISCUSSION OF MICROSCOPIC INVESTIGATIONS:

HIGH SPEED IMPACT PHENOMENA

Detailed stereo microscope investigations demonstrated that lunar microcraters of the sizes observed are characterized by a central glass-lined pit, a lightened zone of shock-fractured minerals, and a spall area roughly 4.5 times larger in diameter than the central pit. Hence they have geometries similar to craters produced in the laboratory. The presence of a glass-lined pit indicates impact velocities in excess of 10 km/sec.

Gault et al (1968) demonstrated that ejecta during the initial phases ("jetting") of a large-scale impact event may well reach absolute velocities exceeding the projectile's impact velocity by a factor of 1.5 to 3. However relative velocities in excess of 10 km of fine-grained particles within any given ejecta plume are difficult to justify from considerations of cratering mechanics. Our present knowledge from laboratory experiments indicates a highly organized ejecta trajectory distribution. Large scale crossing

of ejecta trajectories is not observed, especially during jetting. Consequently relative velocities have to be small. We therefore believe that all glass lined pits (which account for $\approx 90\%$ of the cratering phenomena observed) are due to collisions with high speed, primary cosmic particles.

This hypothesis is further supported by the presence of sharp demarcation lines between heavily cratered and completely uncratered areas on rock 12017, 12051, 12038, 12021 (Figure 23). If the uncratered areas were just freshly broken surfaces, the demarcation line would be strongly controlled by the rock's shape, i.e. the line would be formed by sharp edges, corners, etc. The demarcation line however in all 4 rocks runs across relatively flat surfaces irrespective of rock geometry (Figure 24). It can be traced over the whole circumference of the rock and clearly represents a plane rather than a line separating cratered and uncratered areas. Such a crater distribution is incompatible with in-flight collisions of fine. grained secondary ejecta; there is no basis to assume that rocks do not tumble during large scale ejection. Even granting that they do not, one has certainly to postulate that they orient themselves according to their aerodynamically most stable configuration. This could not be observed in any of the 4 cases.

The spatial distribution of cratered and uncratered surfaces therefore cannot be explained by in-flight collisions. The rock must have been at rest and was sitting on the lunar surface. Parts of it were buried in the regolith and cut off from impacting projec-

tiles, be they primary or secondary ones. The buried parts are uncratered. Such an explanation is further strengthened by the concentration of ropy splashes around the soil line. With the rock at rest, the majority of secondary projectiles however does not impact at velocities high enough to cause glass lined pits. The majority of secondary projectiles will impact at speeds lower than lunar escape velocity, i.e. lower than 2.2 km/sec. Consequently the glass lined pits are due to impacts of high speed, primary cosmic particles.

It is conceivable however to attribute some few pits to genuine secondary high speed ejecta. Such pits are probably the results of small cratering events happening close to the rock. The rock could have blocked part of the ejecta at full speed. Craters of such an origin obviously require extremely special geometrical arrangements of impact site and rock geometry. They therefore must be classified as rare exceptions.

Likely craters with such an origin are those displaying dark brown glass linings which are unrelated to the composition of target minerals. The glass color is similar to that of big glass coatings and thus we conclude that it was derived from the lunar soil. The craters reported by Mason et al. (1970) must also be classified in this category. Mason et. al.'s chemical analyses of glass linings indicate lunar soil composition.

LOW SPEED IMPACT PHENOMENA

Only about 10% of all features observed can be attributed to low speed projectiles and thus possibly to secondary ejecta. Such

features are pitless craters, glass coatings, ropy splashes and welded dust. Their impact energies were not sufficient to melt the target rock; the highest shock damage observed is intense micro-fracturing especially of plagioclase. At present no detailed optical or x-ray studies are available to estimate absolute peak shock pressures for the production of halo material. Such pressures can be as high as 300 kb or as low as 50 kb. Consequently maximum impact velocities can range from a few hundred meters/sec to 3 km/sec.

The collisions of the rock with projectiles causing pitless craters or with glass masses producing glass coatings can occur either in flight or on the lunar surface. Ropy splashes and welded dust however are deposited while the rock is resting on the lunar surface. This is indicated by their concentration around the demarcation line of cratered and uncratered rock surfaces on rocks 12021, 12038 and 12051. Ropy splashes and welded dust however can potentially be encountered on all cratered surfaces; never have they been observed on uncratered surfaces. This again indicates that the uncratered rock part was buried in the soil.

"Frosting" was described as lack of vitreous luster of crystal faces. It is always present over the entire uncratered surfaces and virtually absent on cratered ones. Its origin is tentatively ascribed to sandblasting effects of exceedingly small secondary particles during ejection of the rock. The mass removal is virtually negligible as indicated by intact crystal faces, sharp corners, etc. Due to the partial burial of the rock, the frosting was protected from destruction by micrometeorite bombardment. Some vug minerals on the cratered surfaces still display the original

frosting; those which are not frosted are probably in vugs which were freshly exposed to the rock surface due to cosmic erosion.

CHARACTER OF COSMIC EROSION

Under "cosmic erosion" we understand the gradual wearing away of rock surfaces due to spallation processes caused by the interaction of shock waves with the free surfaces of rocks as well as the catastrophic rupture and breakup of entire rocks (Shoemaker et al., 1970, Gault and Wedekind, 1969). Both processes could be observed on the rocks.

The gradual wearing away of rocks is readily seen on all cratered surfaces. The dominant process on the scale observed is by far the catastrophic spallation of rock surfaces due to discrete microcratering events. Individual events responsible for complete or partial removal of surface promontories are easily identified. Overlapping spall zones are common which lead to partial or complete destruction of pit craters. Discrete segments of pit walls are broken off indicating a catastrophic rather than gradual removal of material. In large diameter spall zones the presence of halo material outside the central halo zone demonstrates the catastrophic removal of entire craters. The great proponderance of these "catastrophic" spallation features indicates that the gradual wearing away of lunar rock surfaces is dominated by discrete high velocity, high energy impacts.

The extremely shiny surfaces of glass coatings seem to demonstrate that removal of rock surfaces due to low energy projectiles does not

exist on a significant scale. Similar observations were made on large single crystal faces as well as on the glass linings of central pits. If such a "sandblasting" effect of secondary projectiles were of importance, some of the glass coatings, single crystal faces or glass linings would be exposed to the surface long enough to be densely pitted, chipped and "frosted". This however was rarely observed. Consequently the state of preservation of glass and single crystal surfaces supports the view that secondary "sandblasting" is of little importance for spallation processes on the moon. The gradual wearing away of rocks (on the scale observed) appears to be dominated by catastrophic rupture and destruction due to discrete micrometeorite impacts.

The catastrophic rupture of entire rocks was observed on rock 12073, where an exceptionally large impact event was split in half by a freshly broken rock surface. The remaining half was not returned by the astronauts. In addition large craters on other rock surfaces clearly display radial patterns of microcracks extending up to 10 crater radii (Figure 25).

CRATER STATISTICS:

OBSERVATIONS

Differences in crater populations on different surfaces of one rock are readily observed with the naked eye. An abundance of halo material increases the albedo of the rock so that, in general, the "lighter" surfaces are more heavily cratered than the darker ones. Under the microscope, however, it is evident that for any given rock surface, the absolute crater counts can vary considerably from one field of view to the next (our field of view was 1.25 cm in diameter). Recent, relatively large, impact events may have erased the entire record of the smaller crater populations; consequently some fields of view abound in small craters while others lack them completely. It is not possible, therefore, to characterize the crater population of a surface on the basis of a single field of view. For the same reason it is impossible to define the limits of a rock surface containing a distinctive crater population on the basis of microscopic crater counts only. Hence, for each rock, we selected areas which contained distinct crater populations based on macroscopic halo material distribution, the shape of the rock, and the presence of a glass coating. Each of these surfaces was evaluated separately. Areal corrections for cracks, vugs and other extreme topography were made to obtain the surface actually exposed to the meteoritic environment.

Within a given population, i.e. a selected rock surface area, the craters were further classified according to their diameters.

Measurements of pit diameters are summarized in Table 1. A factor of 4.5 was used to convert from pit diameter into spall diameter in order to derive the cumulative size - frequency distributions of the true crater diameters on crystalline and breccia surfaces as illustrated in Fig. 26 and 27. Spall diameters were measured directly on the glass coatings (Surface II, rock 12017 and Surface III, rock 12073). The error bars are based on the square root of the sum of all craters larger than a given size class.

INTERPRETATIONS

The cumulative frequency curves presented in Fig. 26 and 27 are characterized by a systematic flattening in the range of the smaller craters, a steepening in the range of the larger craters and a region of intermediate sized craters with slopes of about -2. These distributions have many similarities with crater populations larger than a meter that are expressed on the lunar surface (Shoemaker et. al. 1969, 1970, Hartmann, 1970, Oberbeck and Quaide, 1968, Gault, 1970, Ronca and Green, 1970 and many others). However, specific problems related to micrometeorite impact occasionally seem to prevent analogous interpretations.

Small Craters:

The flattening of the cumulative curves (Fig. 26 and 27) represents a relative decrease in the frequency of the smallest craters.

Two explanations are possible

a) The flattening is an artifact similar to that observed in large scale crater counts on the lunar surface (Gault, 1969, Shoemaker et. al., 1970). It indicates that we failed to record the smallest crater sizes in a quantitative way; this is due to problems in recognizing small glass lined pits which reflect light in a way similar to fractured crystals and which are colored essentially the same as the host crystal.

b) The flattening reflects a genuine relative decrease in the contribution of smaller craters (=cosmic particles) to the overall populations.

The recognition problem when viewing glass coated surfaces is virtually eliminated because the smooth, shiny glass surfaces permit ideal observational conditions. Because the "glass curves" remain straight down to crater sizes much smaller than those corresponding to curve flattening on the other surfaces, we conclude that the flattening of the crater populations on breccia and crystalline rocks represents an artificially introduced deficiency in smaller craters. However, we attribute the curve flattening of the glass populations (at least in part) to a genuine decrease in the relative number of cosmic particles, because the flattening occurs at crater sizes well above the recognition and resolution level for glass coatings.

Large Craters:

The cumulative curves for craters larger than about 4 - 5 mm (Fig. 26 and 27) display a steepening which results in an approximate slope of -3. This steepening can again be explained in various ways.

a) The steepening of a curve at larger crater sizes may indicate a "production" distribution, i.e. a direct record of craters produced on a rock surface since that surface was first exposed to the meteoritic environment. Gault (1970) and Shoemaker et. al., (1970) have shown that such a "production" curve may be characterized by a slope of about -3 (see Fig. 26).

b) Gault and Wedekind (1969) demonstrated experimentally the break up of rocks due to micrometeorite impact. There is always a maximum crater size which can possibly be observed on a given rock because a slightly more energetic event would have completely ruptured the specimen. The combined energy of several cratering events, none of which alone would rupture the rock, results also in the destruction of the rock. In a statistical sense, rocks on the lunar surface which experienced an excess of these events are destroyed. Those which experienced relatively fewer events remain intact and were ultimately collected. Thus, the rocks returned should have a shortage of large craters.

c) Projectiles not quite energetic enough to break up a rock are capable of producing cracks and fractures along which eventually the rock will break, resulting in the "destruction" of these craters. Thus, there is a genuine trend to lose the record of large craters.

The present quality of our statistical data for the larger craters does not permit firm conclusions to be drawn.

Intermediate Craters:

A slope of about -2 characterizes the cumulative frequency curves for intermediate crater sizes. This slope is constant and independent of absolute crater density (Fig. 26 and 27). It is not clear whether the -2 slope is significant or merely a necessary transition between slopes of -3 (large craters) and slopes much flatter than -2 (small craters). The latter interpretation is suggested for rock surfaces 12006 I and II, 12017 II, 12021 I and II, 12038 I and II, 12051 II and III and 12073 III.

Though this explanation may also hold for the remaining populations, we strongly suggest for these an interpretation analogous to large scale crater counts on the lunar surface. A slope of -2 defines Gault's (1970) "equilibrium" conditions and is in agreement with Shoemaker et. al.'s (1969) "steady state" distribution. Both concepts imply that—given sufficient geological time—distinct crater populations will neither change their size-frequency relations nor their

absolute crater densities because craters are being modified and destroyed at the same rate that fresh craters are being produced. As a measure of crater density, Gault (1970) introduced the concept of "saturation". Saturation is defined as the number of hexagonal close packed circles of a given size that will fit in a given unit area. Crater densities of "equilibrium" or "steady state" populations of large lunar surface craters range typically from 3 to 6% of the saturation value.

Based on these investigations, we consider crater densities of more than 5% saturation as equilibrated rock surfaces. At least one selected surface on each rock possesses a crater population near 10% saturation for craters up to 3 - 5 mm. Thus, we consider rock surfaces 12006 III, 12017 I, 12021 III and IV, 12038 III and IV, 12047 I and II, 12051 I, IV and V, 12073 I and II in equilibrium for intermediate size craters. The densities of our equilibrated surfaces are compared with large scale crater counts in Fig. 28. The agreement serves to confirm the equilibrium nature of the above surfaces.

Another important conclusion results from the crater density coefficient, i.e. from the percentage of saturation. Marcus (1970) pointed out, that large crater density coefficients imply crater destruction predominantly by obliteration and superposition of cratering events while smaller values indicate a significant contribution to crater destruction from small scale sandblasting and ballistic sedimentation. Our anomalously high saturation values (10%) therefore support

our conclusion based on optical observations, i.e. the dominant rock erosion process is due to obliteration and superposition of discrete cratering events. Sandblasting seems to play a minor role only; ballistic sedimentation can be completely excluded.

Mass Distributions of Cosmic Particles:

The glass coated surfaces of rock 12017 and 12073 are clearly not in equilibrium. Thus, they reflect the direct record of craters produced since they were exposed to the meteoritic environment. They are genuine "production" surfaces. Due to ideal observational conditions they are the most suitable surfaces investigated which allow a comparison between microcrater populations and the interplanetary particle flux.

We used the following approach to relate crater diameter with projectile mass: one of us (DEG) found empirically that ejecta mass and projectile kinetic energy are related by

$$M_e = 10^{-10} E^{1.12} \qquad (1)$$

where M_e is mass ejected in grams and E is the required kinetic energy in ergs. This relationship is valid for dense rocks only and does not apply for target materials of vastly different mechanical properties like metals or loose sand. The relationship holds for an impact kinetic energy range from 10^0 to 10^{12} ergs. By using equation (1) and assuming a conical crater with a diameter to depth ratio of 8,

a target rock density of 3.2 gm/cm^3 and an impact velocity of 20 km/sec we derived a relationship between the crater diameter, D, in cm and the impacting particle mass, m, in gm.

$$D = 10^{1.591}m^{.373} \text{ or } m = 10^{-4.265}D^{2.681} \quad (2)$$

The mass distributions obtained may be compared directly with similar distributions based on satellite-borne flux measuring experiments. Figure 29 shows a summary of recently obtained flux data from various sources. Because no independent exposure time data has been obtained for our glass surfaces, the insert of our data is completely arbitrary with respect to the abscissa. However, the relative mass distributions calculated via cratercounts agree with those from other techniques. Our data support the view that there is a genuine relative decrease of cosmic particles with masses less than 10^{-7} to 10^{-8} g.

Flux Dependent Implications

The following section* presents an attempt to calculate exposure and equilibration times for specific surfaces, survival times of rocks and erosion rates on the lunar surface.

These calculations are essentially independent from our crater counts because we only contributed to the confirmation of relative abundances of masses. We did not contribute to the true flux, i.e. to

---

(*) A more detailed version of this section is in preparation. Consequently, we purposely omit the discussion of pertinent data generated elsewhere.

the time parameter, which is the most crucial one in these calculations. Thus, our calculations depend heavily on the reliability of the flux assumed. In addition, we assume constant flux for the times under consideration. Furthermore, the analyses have not considered the true rock exposure geometry; we assumed ideal spheres or ellipsoids, whatever seemed to be the most appropriate judging from the rock's shape. We also postulate that the rock was never buried in the lunar soil, i.e. it was constantly exposed to the meteoritic environment. The solid angle of exposure of the rock surface studied is probably less than 2π steradians. We also did not account for the gravitational concentration of particles at the lunar surface. Considering all these uncertainties, we estimate our results to differ within a factor of 10 from the true values and most likely within a factor of 5.

It is significant to our calculations that the mass distribution indicated in Fig. 29 cannot be described by a single valued function, but that the slope of the distribution changes drastically in the mass range 10^{-7} to 10^{-8} g. For present purposes, the two segments (Fig. 29) may be expressed (cgs units):

$$N = 10^{-18.9}\, m^{-1.2} \quad \left| \; m \geq 10^{-7.2} \text{ g} \right. \qquad (3)$$

$$N = 10^{-14.1}\, m^{-.53} \quad \left| \; m \leq 10^{-7.2} \text{ g} \right. \qquad (4)$$

Thus, with an assumed average impact velocity of 20 km/sec equation (3) and (4) can be recast using equation (2) into

$$N = 10^{-0.27} D^{-3.21} \quad D \geq 0.8 \text{ mm} \qquad (5)$$

$$N = 10^{1.80} D^{-1.42} \quad D \leq 0.8 \text{ mm} \qquad (6)$$

where now N is given as the number of craters equal to or larger than diameter D (cm) that are formed per cm^2 in 10^6 years.

Equations (4) and (5) are presented in Figure 30. Also presented are the conditions for saturation and various percentages of saturation. The combination of Figs. 26, 27, and 30 indicates that equilibrium crater distributions (10% saturation) can be attained on the rock surfaces in less than 10^5 years. Indeed, the calculations suggest that beginning at 10^4 years, equilibrium is first obtained for craters 0.8 mm diameter and then spreads to smaller and larger diameters with increasing time. At 10^5 years, craters smaller than about 5 mm that we have observed would have attained equilibrium. For glass surface 12017 II a minimum "exposure" age of 10^3 years is obtained.

Long"meteoritic"exposure ages permit the formation of craters so large that the impacts totally rupture the rock; such catastrophic destruction of rocks precludes very long cosmic ray exposure ages. The equation 6 of Gault and Wedekind, 1969, together with a rupture energy of 7×10^6 ergs/gram based on unpublished data by one of us (DEG) for crystalline rocks, permit to calculate the mean survival time before catastrophic rupture for the seven rocks we examined. The results are given in Table II. In all cases, the survival times are larger than the time required to attain equilibrium conditions

for intermediate sized craters. This lends additional support that most of the surfaces observed are truly equilibrated.

By combining the breakup energy for various rocks, their survival time and equation (1) it is possible to determine the mass and thus the volume (d=3.2g (cc) of material removed from the surface of the rock just prior to rupture. The corresponding erosion rate obtained is about .2 to .4 mm per 10^6 years; this is considered a lower limit.

ACKNOWLEDGEMENTS:

We acknowledge the hospitality of the Lunar Science Institute which is administered by the Universities Space Research Association under NASA grant NSR-09-012-071. We appreciate the cooperation of curator D. H. Anderson, R. L. Laughon and other staff members of the Lunar Receiving Laboratory. J. F. Vedder, NASA-Ames allowed us to quote his unpublished results on high speed microparticle cratering.

REFERENCES:

Alexander, W. M., Corbin, J. D., Arthur, C. W. and Bohn, J. L., Lunar Explorer 35: 1967-1968 Measurements of Picogram Dust Particle Flux in Selenocentric Space. Twelfth COSPAR Meeting, Prague, 1969.

Berg, O., Personal Communication (1970).

Carter, J. L. and MacGregor, J. D., Mineralogy, Petrology and Surface Features of some Apollo 11 Samples. Proceed. Apollo 11 Lunar Science Conference, Vol. 1, 247-265, 1970.

Dietz, E. D. and Vergano, P. J., Origin of Glass Deposits in Lunar Craters, Science, 168, 609-610, 1970.

Engelhardt, W. V., Arndt, J., Müller, W. F., and Stöffler, D., Shock Metamorphism in Lunar Samples and Origin of the Regolith at the Apollo 11 Landing Site, Proceed. Apollo 11 Lunar Science Conference, Vol. 1, 363-384, 1970.

Gault, D. E., Saturation and Equilibrium Conditions for Impact Cratering on the Lunar Surface: Criteria and Implications, Radio Science, 5, 273-291, 1970.

Gault, D. E. and Wedekind, J. A., The Destruction of Tektites by Micrometeorite Impact, J. Geophys. Res. 74, 27, 6780-6794, 1969.

Gault, D. E., Quaide, W. L., Oberbeck, V. R. Impact Cratering Mechanics and Structures; in: Shock Metamorphism of Natural Materials, French, B. M., and Short, N. M. Editors, Mono Book Corp., Baltimore, Md. p. 87-99, 1968.

Gürtler, C. A. and Grew, G. W., Meteroid Hazard Near the Moon, Science 161, 462, 1968.

Gold, T., Apollo 11 Observations of a Remarkable Glazing Phenomenon on the Lunar Surface. Science, 165, 1345-1349, 1969.

Gold, T., Origin of Glass Deposits in Lunar Craters, Science 168, 611, 1970.

Green, J., Origin of Glass Deposits in Lunar Craters, Science 168, 608-609, 1970.

Greenwood, W. R. and Heiken, G., Origin of Glass Deposits in Lunar Craters, Science 168, 610-611, 1970.

Hartmann, W. K., Preliminary Note on the Lunar Cratering Rates and Absolute Time Scales, Icarus 12, 131-133, 1970.

Hörz, F., Structural and Mineralogical Evaluation of an Experimentally Produced Impact Crater in Granite, Contr. Mineral. and Petrol., 21, 365-377, 1969.

Lunar Sample Preliminary Examination Team, Preliminary Examination of Lunar Samples from Apollo 11, Science, 165, 1211-1227, 1969.

Lunar Sample Preliminary Examination Team, Preliminary Examination of Lunar Samples from Apollo 12, Science, 167, 1325-1339, 1970.

Marcus, A. H., Comparison of Equilibrium Size Distribution of Lunar Craters J. Geophys. Res. 75, 4977-4984, 1970.

Mason, B., Fredriksson, K., Henderson, E. P., Jarosewich, E., Melson, W. G., Towe, K. M. and White, J. S. Mineralogy and Petrology of Lunar Samples, Proceed. Apollo 11 Lunar Science Conference, Vol. 1, 655-660, 1970.

McKay, D. S., Greenwood, W. R., and Morrison, D. A., Origin of Small Lunar Particles and Breccia from the Apollo 11 Site, Proceed. Apollo 11 Lunar Science Conference, Vol. 1, 673-694, 1970.

Moore, H. J., Gault, D. E. and Lugn, R. V., Experimental Impact Craters in Basalt, Trans. Mining Engrs., 258-262, 1963.

Naumann, R. J., The Near Earth Meteroid Environment, NASA TN D-3713, 1966.

Naumann, R. J., Jex, D. W., and Johnson, C. L., Calibration of Pegasus and Explorer XXIII detector panels, NASA, TR R-321, 1969.

Neukum, G., Mehl, A., Fechtig, H., and Zähringer, J., Impact Phenomena of Micrometeorites on Lunar Surface Materials, Earth and Plan. Science Letters 8, 31-35, 1970.

Oberbeck, V. R., and Quaide, W. L., Genetic Implications of Lunar Regolith thickness Variations, Icarus, 9, 446-465, 1968.

Ronca, L. B. and Green, R. R., Statistical Geomorphology of the Lunar Surface Geol. Soc. of Am. Bull. 81, 337-352, 1970.

Shoemaker, E. M., Batson, R. M., Holt, H. E., Morris, E. C., Rennilson, J. J., and Whitaker, E. A., Observations of the Lunar Regolith and the Earth from the Television Camera on Surveyor 7, J. Geophys. Res. 74, 6081-6119, 1969.

Shoemaker, E. M., Hait, M. H., Swann, G. A., Schleicher, D. L., Schaber, R. L., Sutton, R. L., Dahlem, D. H., Goddard, E. N., Waters, A. C., Origin of the Lunar Regolith at Tranquility Base, Proceed. Apollo 11 Lunar Science Conference, Vol. 3, 2399-2412, 1970.

Soderblom, L. A., A Model for Lunar Impact Erosion Applied to the Lunar Surface, J. Geophys. Res. 75, 2655-2661, 1970.

Vedder, J. F. (unpublished data) 1970.

Insert:

McKay, D. S. (1970) Microcraters in Lunar Samples Proceedings of the Electron Microscopy Society of America; C. V. Arceneauk, ed. (1970)

FIGURE CAPTIONS:

Fig. 1: Typical views of rock specimens investigated. Note: glass coatings on rocks 12017 and 12073 (on bottom of rock). Length of bar: 3 cm.

Fig. 2: Close up of cratered rock surface (rock 12017). Note: abundance of craters (black, shiny dots surrounded by white halo material). Scale is in cm.

Fig. 3: Schematic cross section through microcrater. (Definitions: "Pit": glass lined cavity in the center of overall crater; "pit-depth": distance from glass rim (fresh or broken) to bottom of pit; "halo": concentric area around pit characterized by different albedo due to shock induced microfracturing; "spall": concentric area around pit which was removed due to shock wave interaction with the free surface; (spall diameter = crater diameter).

Fig. 4a (left): Microcrater with central pit and spall zone on breccia 12073. Note: breccias do not display prominent halo zones; cracks and spall fractures within spall zone display characteristic radial patterns.

4b (right): Microcrater with central pit, halo zone and spall area on crystalline surface (rock 12047). Note: halo zone is especially enhanced by plagioclase crystals.

Fig. 5a (left): Close up of glass lined pit (rock 12051). Note: highly circular outline of pit and hummocky relief of glass lining. Pit has slightly raised rim.

5b (right): Close up of glass lined pit (rock 12051). Note: highly irregular outline of pit which has no raised rim; halo zone is prominent.

Fig. 6: Close up of glass lined pit. Note: highly hummocky surface relief of glass lining and absence of raised crater lip; i.e. the glass "flowed" onto the surface.

Fig. 7: Highly idealized cross sections through microcraters, outlining various types of spall plate geometries. All transitions between these cases have been observed.

Fig. 8: Close up of "stylus" pit (rock 12051). Note: glass lined pit sits on pedestal above crater floor; spall zone associated with this event is still visible.

Fig. 9: Highly idealized cross sections through "stylus" craters. All transitions between these cases have been observed.

Fig. 10: Size frequency histogram of measured pit diameters on crystalline rocks (3813 measurements).

Fig. 11: Ratios of spall/pit diameter (D_S/D_P) and halo/pit diameters (D_H/D_P) versus count frequencies.

Fig. 12: Size frequency histogram of measured pit diameters on breccia 12073 (734 measurements).

Fig. 13: Microcraters (arrows) on glass coating of rock 12073. Note: high circularity of central pits as well as spall zones. (V,C = vesicles, partically caved in).

Fig. 14: Size-frequency histogram of measured spall diameters on glass surfaces (rocks 12073 and 12017; 187 measurements).

Fig. 15: Spallation of glass coating due to large micrometeorite impact on rock 12054.

Fig. 16: Cross sections through craters formed by low speed impact. The rippled zone indicates lateral extension of halo material. Types b and c are the most common ones.

Fig. 17: Glass coating on rock 12017. Note the perfect preservation of the glass surface. The presence of schlieren (right) indicates shock melting. Tear drop shaped splashes of a somewhat darker glass indicate a second generation of glass splashes.

Fig. 18: Contact of glass coating and crystalline substrate (rock 12017) (H = halo material; G = glass splashes and drops associated with the deposition of the main glass coating).

Fig. 19: Ropy splashes (R) on rock 12051. Note the highly irregular outline of these features, the small halo zone associated with them and their hummocky, dusty appearing surface.

Fig. 20: Ropy splashes (R) and welded dust (W) on rock 12051. Note the genetic relationship between these two features, i.e. welded dust is a thinner version of ropy splashes.

Fig. 21: "Frosting" of single crystal pyroxene face (Rock 12021). Note the absence of vitreous luster typical for fresh crystal surfaces.

Fig. 22: Experimental craters produced by microparticle accelerator.

a) glass target (impact velocity: 11.9 km/sec, Al-projectile of 1.25 μ diameter)

b) oligoclase target (impact velocity: 13.6 km/sec, Al - projectile of .97 μ diameter).

c) Olivine target (impact velocity: 13.1 km/sec, Al - projectile of 1.32 μ diameter).

Fig. 23a: Completely unpitted "bottom" of rock 12051.

23b: Heavily cratered "top" of rock 12051. Arrow indicates largest crater observed; this event is responsible for an extensive fracturing system; it is possible that the curved fracture on the "bottom" side (23a) was generated by that event.

Fig. 24: Demarcation lines between cratered and uncratered surfaces.

a) Rock 12038: left side is "frosted" and was heavily dust covered, indicating burial in the lunar soil; right side is cratered. Note: relatively sharp transition between cratered and uncratered surfaces.

b) Rock 12017: abundant craters on right hand portion of glass coating; no craters were observed on left side.

Fig. 25: Impact event with prominent crack system (extending to upper and lower right hand corners. Note also prominent spall zone. Large crack could not be identified with a discrete event (rock 12073).

Fig. 26: Cumulative frequency distributions of microcraters from 3 selected surfaces of rock 12006. (see text)

Fig. 27: Cumulative frequency distributions of microcraters from selected surfaces of 6 Apollo 12 rocks (see text)

Fig. 28: Size frequency relations and crater densities for macro- and micro-craters. (see text)

Fig. 29: Relative mass distributions and flux of cosmic microparticles obtained from various sources. The mass distributions derived from crater counts are inserted for comparison.

Fig. 30: Cumulative number of craters per cm^2 produced at various times based on assumed flux. Various levels of saturation are included. Exposure and equilibration times can be extropolated by direct comparison with Fig. 26 and 27.

Table I: Measurements for pit diameters on various selected rock surfaces.

Table II: Parameters for calculation of mean lifetime (t_{rm}) for some Apollo 12 rocks. (For more details of calculation see Gault and Wedekind, 1969).

TABLE I

ROCK	SURFACE TYPE [1]	SURFACE DESIGNATION [2]	PIT DIAMETER IN MM															
			.0625	.125	.187	.250	.313	.375	.438	.50	.563	.625	.688	.750-.938	.938-1.250	1.250-1.560	1.560-1.870	1.870-
12006	C	I	105	34	11	11	3	1	3	1	--	--	1	--	--	--	--	--
12006	C	II	39	20	14	9	5	2	3	2	1	--	--	--	--	--	--	--
12006	C	III	81	105	79	49	22	18	8	3	4	1	--	6	2	--	--	--
12017	C	I	n.d.	11	15	9	6	6	3	5	1	4	--	1	1	--	--	--
12017	G	II	n.d.	13	4	4	5	1	4	4	--	4	--	2	1	--	--	--
12038	C	I	89	57	59	33	23	9	5	7	1	5	1	5	2	--	--	--
12038	C	II	53	61	31	20	22	16	13	8	5	5	2	7	2	1	--	--
12038	C	III	1	3	8	6	4	1	--	1	--	2	--	1	--	--	--	--
12038	C	IV	6	5	11	8	5	3	1	5	--	1	2	2	1	--	--	--
12047	C	I	5	21	11	3	8	9	7	8	3	2	5	6	3	--	1	--
12047	C	II	n.d.	38	35	16	19	13	12	12	4	8	4	11	1	0	1	--
12051	C	I	5	35	50	41	33	20	11	14	3	7	8	12	1	1	--	--
12051	C	II	n.d.	16	21	6	10	9	7	7	2	7	2	6	5	2	2	1
12051	C	III	n.d.	25	30	21	14	10	9	4	3	1	1	4	4	2	1	2
12051	C	IV	1	14	8	18	12	6	7	4	4	1	1	4	2	--	--	--
12051	C	V	n.d.	12	11	14	9	1	9	4	6	5	3	2	4	--	--	--
12073	B	I	n.d.	26	43	31	25	12	15	4	6	6	7	9	2	--	--	--
12073	B	II	7	83	57	37	37	27	15	12	8	2	1	4	3	1	1	1
12073	G	III	14	29	32	19	12	8	8	3	2	2	1	3	1	1	--	--
12021	C	I	n.d.	97		122		79		44		23		25	6	3	--	--
12021	C	II	n.d.	37		50		32		9		8		7	5	2	1	--
12021	C	III	n.d.	61		81		63		33		14		9	5	5	2	1
12021	C	IV	n.d.	26		18		5		3		1		1	--	--	--	--

1) C = crystalline, B = breccia, G = glass (note: these are spall diameters on glass coatir

2) These numbers refer to figures 26 and 27

TABLE II

Rock No.	Overall Dimensions (cm)	Mass (grams)	M_1 (micrograms)	M_2 (miligrams)	D max (cm)	t_{rm} (10^6 yrs)
12006	6x6x4	181	6.4	0.21	1.6	0.98
12017	2.5x3x5	53	1.9	0.06	1.0	0.50
12021	8x12x14	1877	67.0	2.2	3.9	3.4
12038	5.5x7.5x12.5	746	26.0	0.86	2.8	2.0
12047	2.5x6x9	193	6.8	0.22	1.7	1.0
12051	7x11.5x16	1660	59.0	1.9	3.8	3.2
12073	6x6x10	408	14.0	0.47	2.2	1.7

1 Assuming average impact velocity of 20 km/sec

M_1 is smallest particle considered effective in contributing to rupture

M_2 is largest particle that could impact rock without causing catastrophic rupture

D_{max} diameter of crater produced by impact of M_2

t_{rm} Mean lifetime of rock before catastrophic rupture by impact of M_2

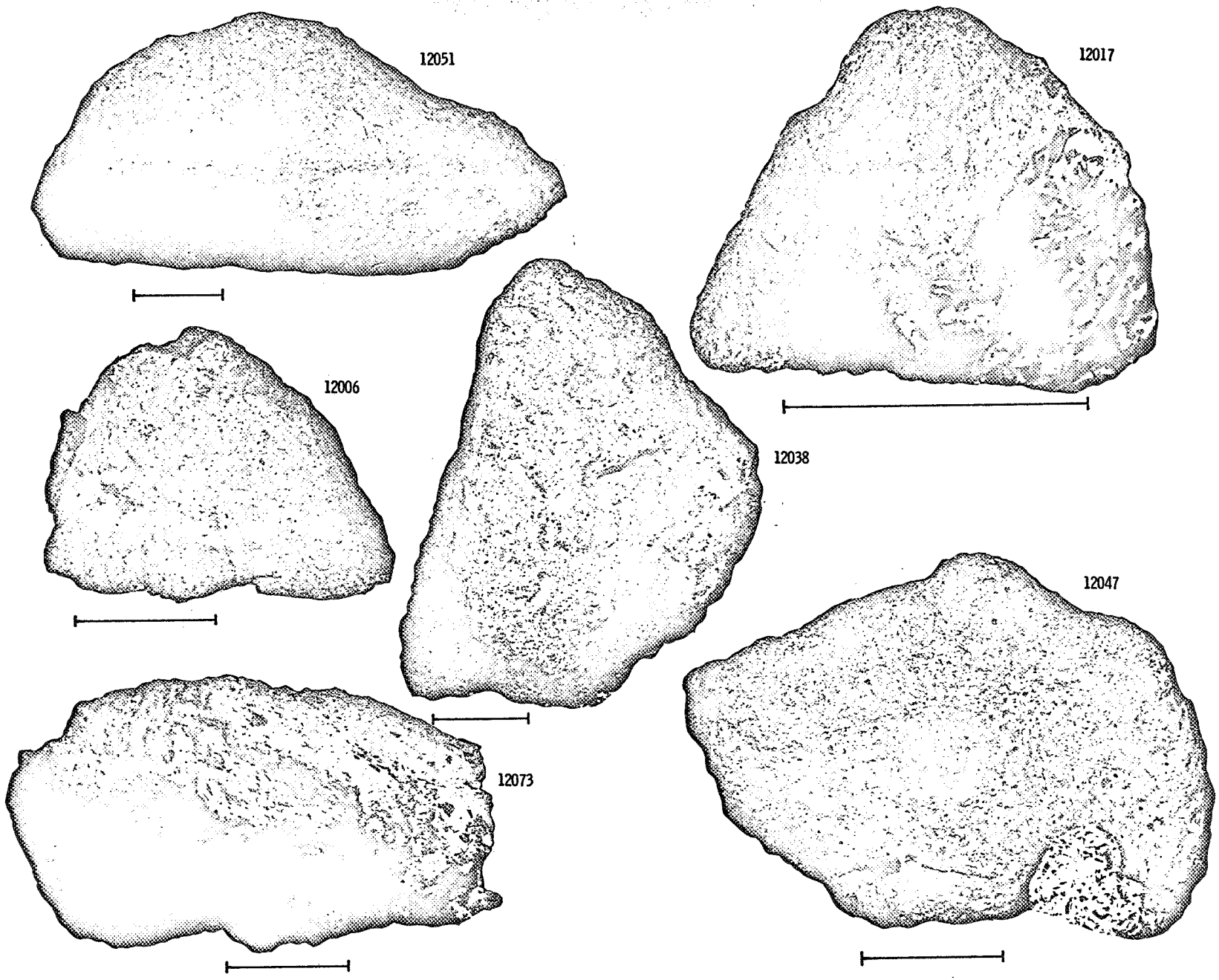

Figure 1

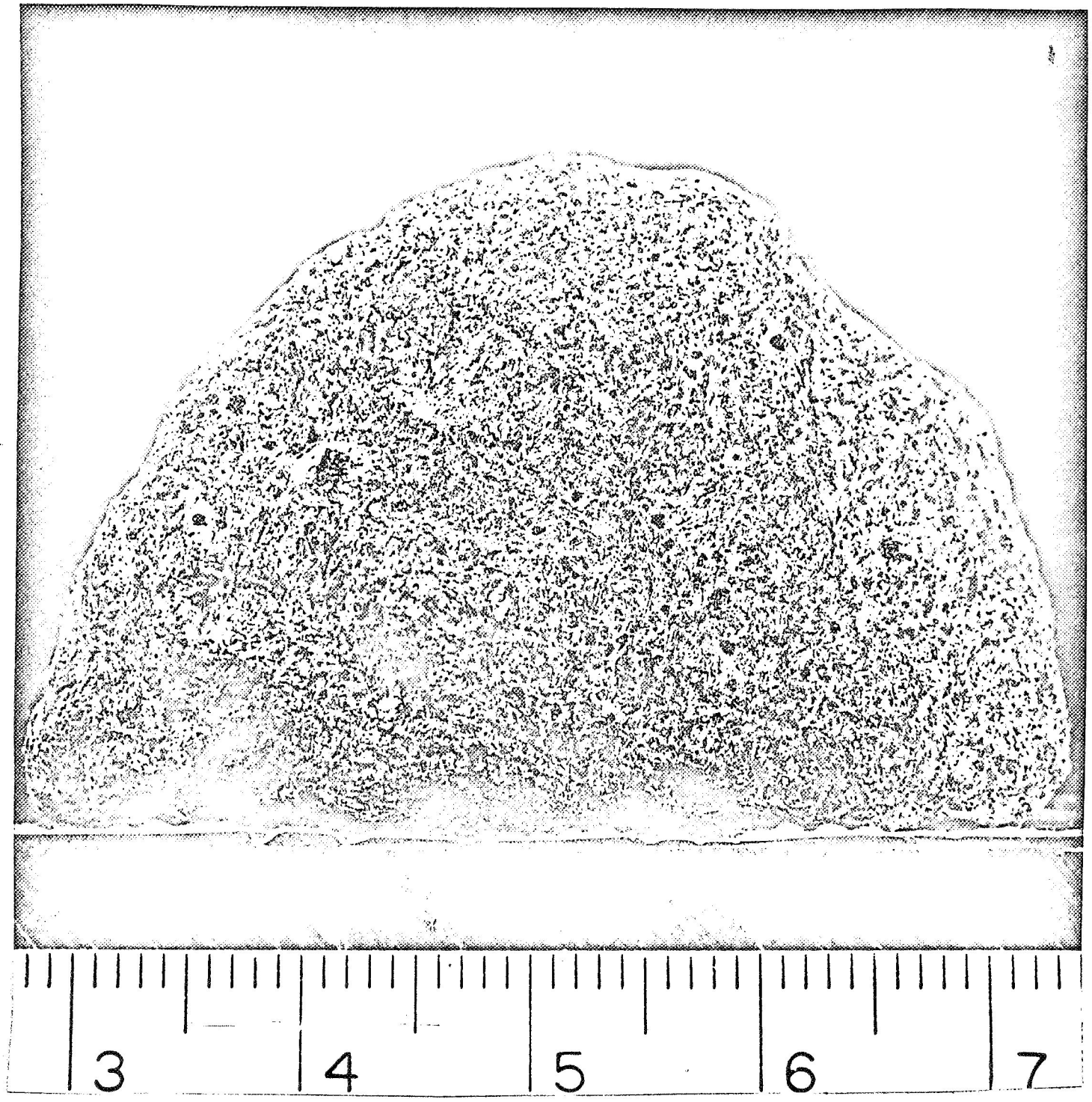

Figure 2

SCHEMATIC OF MICROCRATER

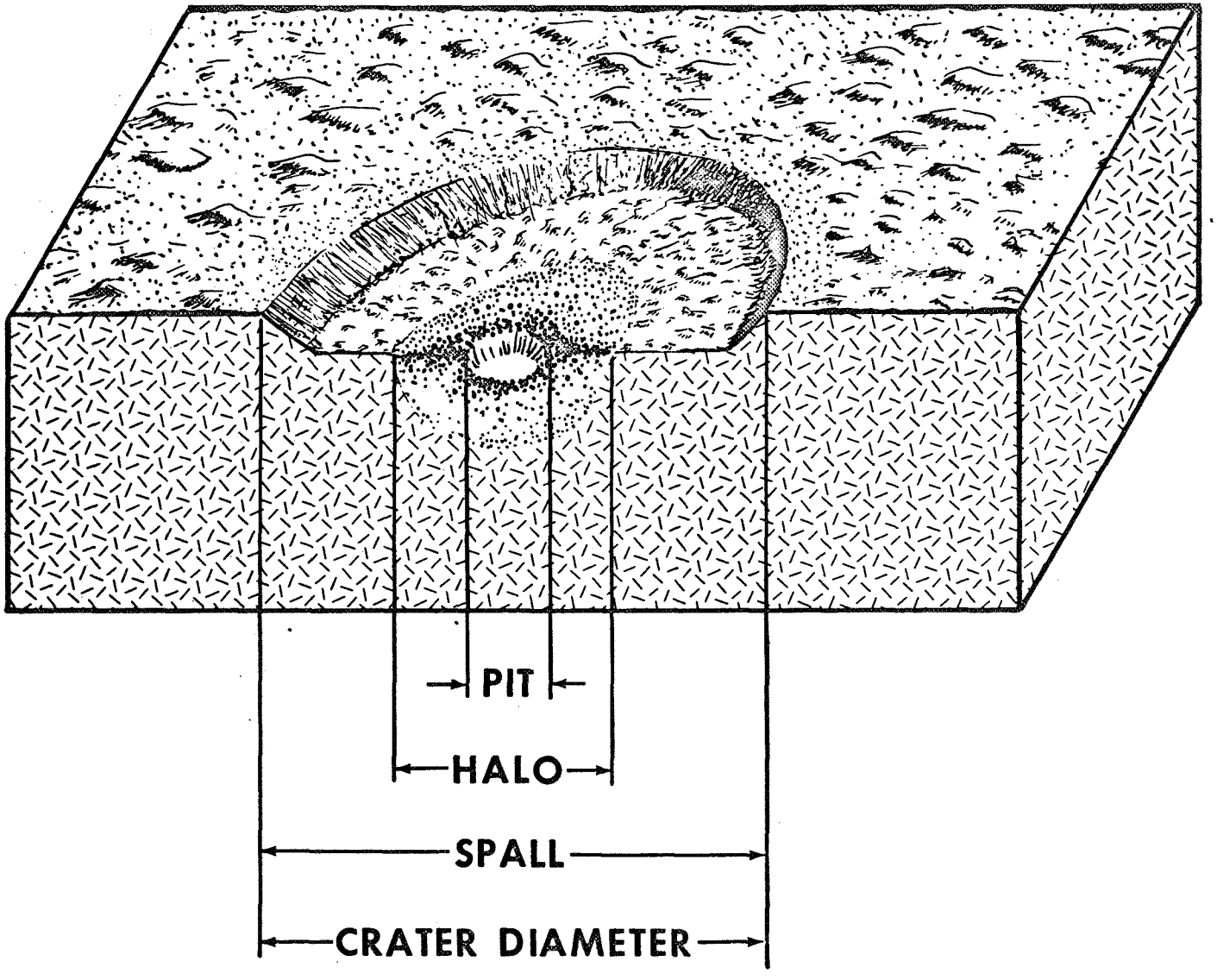

Figure 3

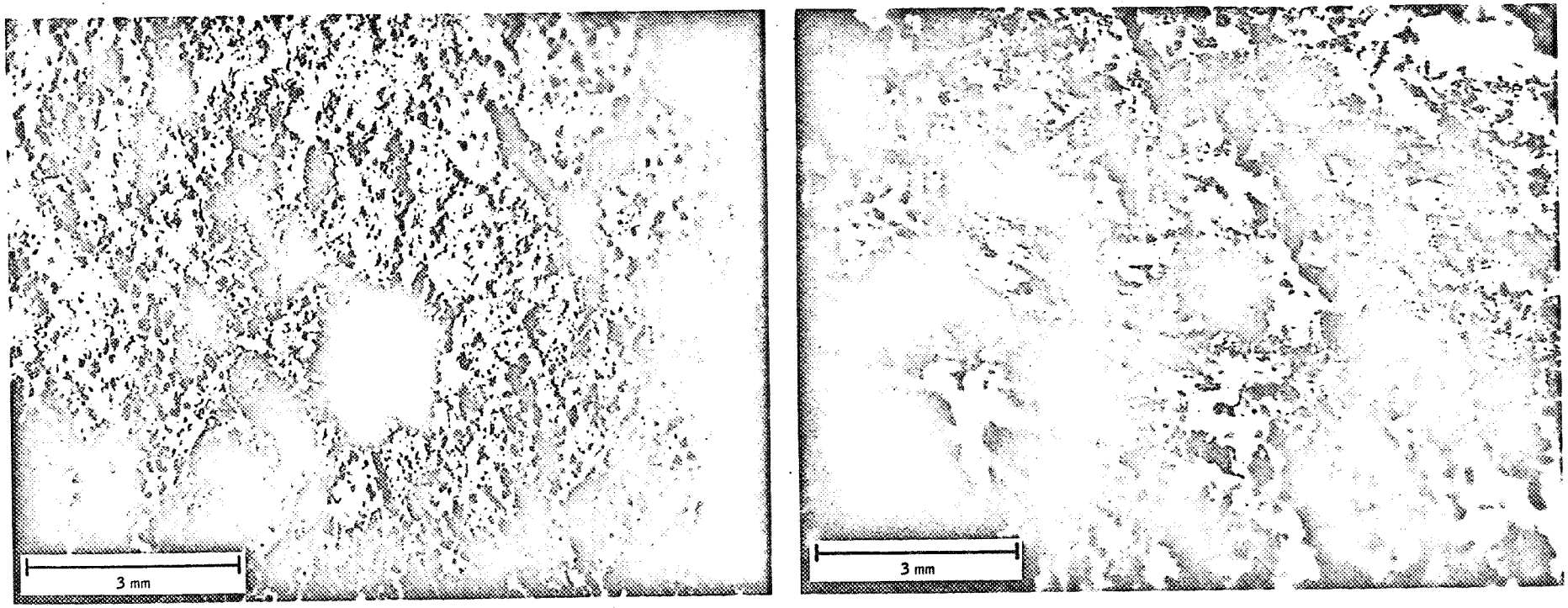

Figure 4

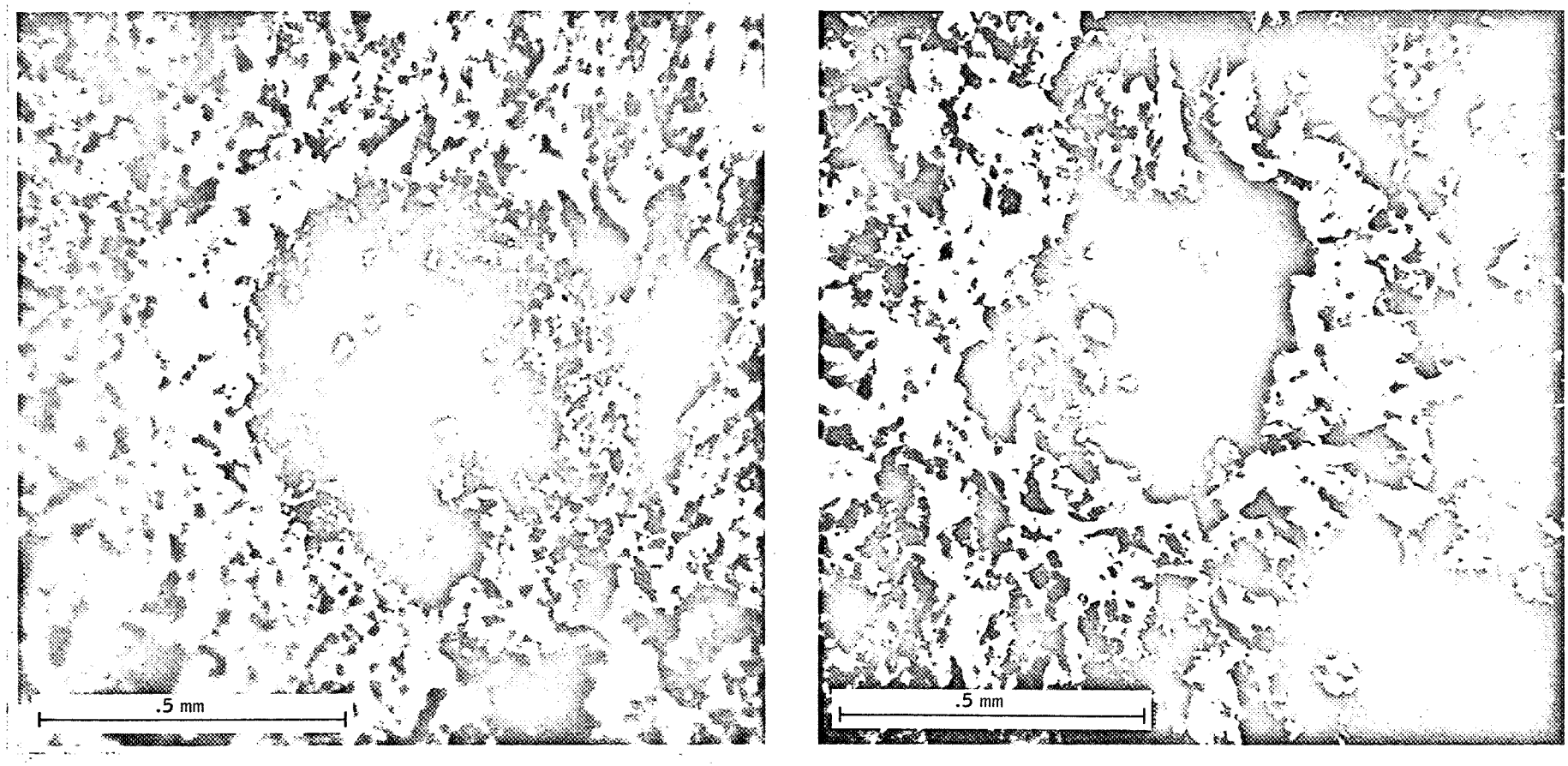

Figure 5

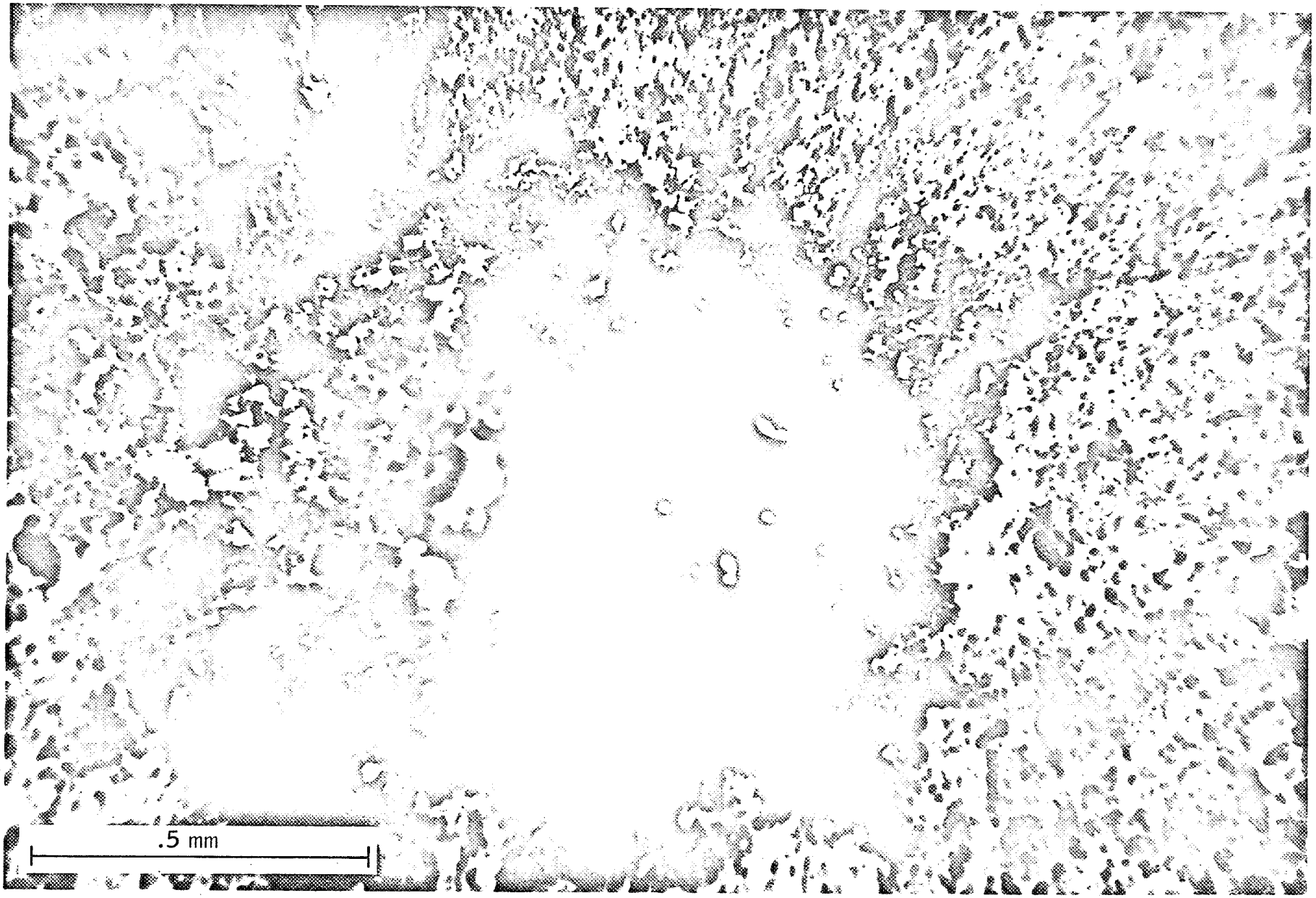

Figure 6

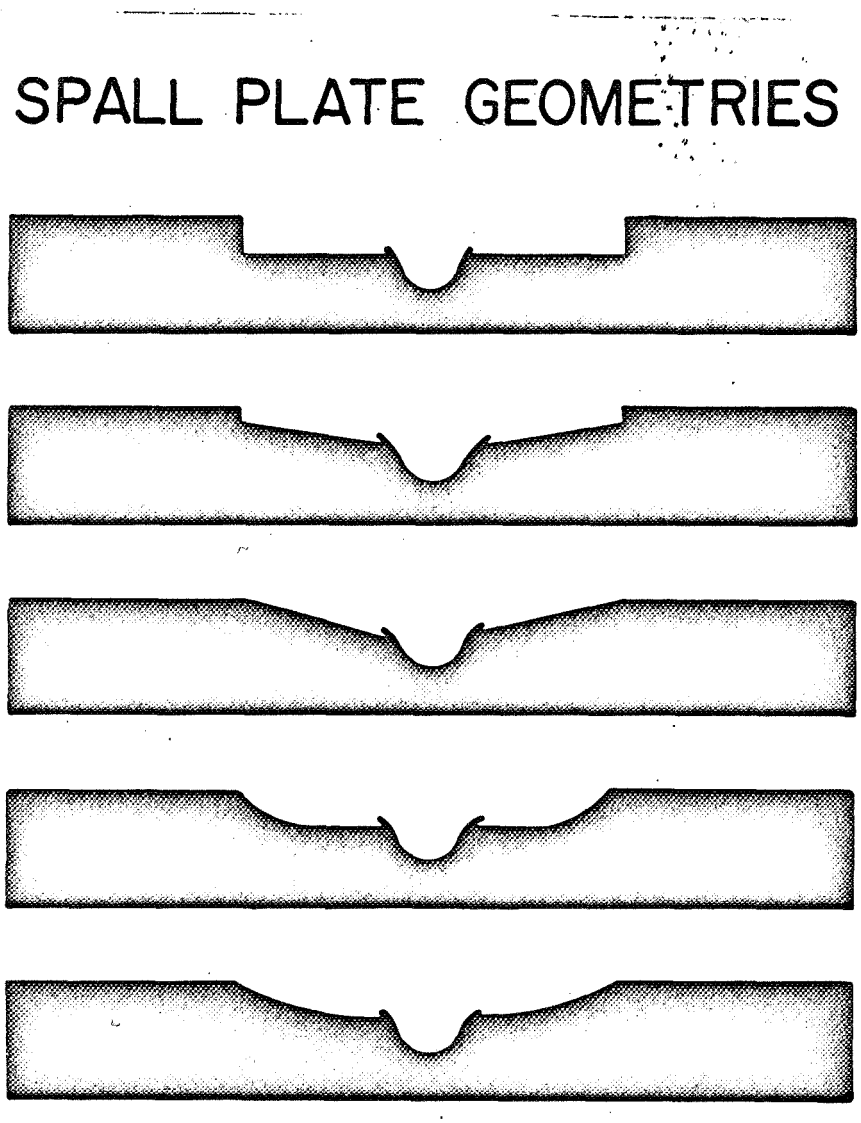

Figure 7

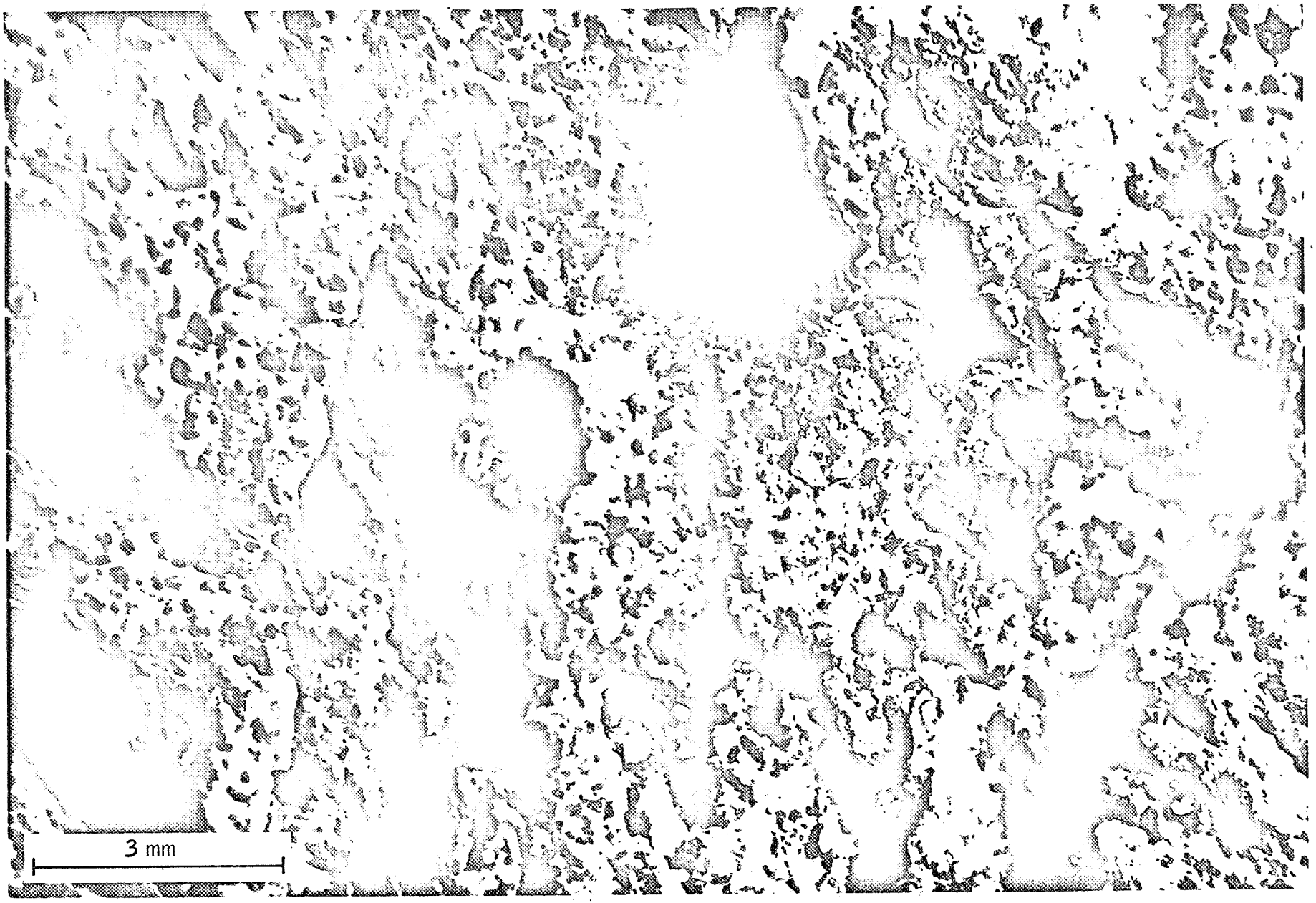

Figure 8

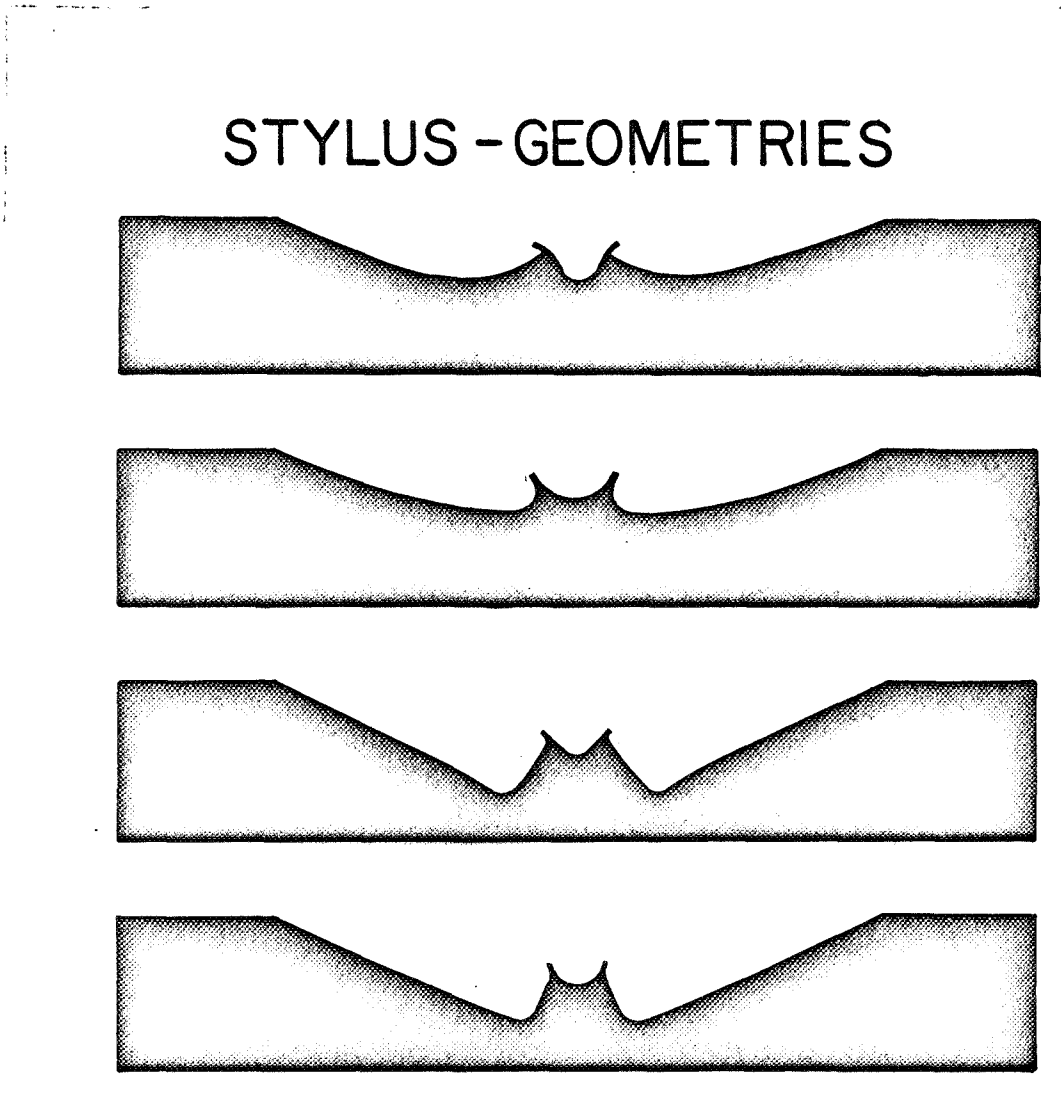

Figure 9

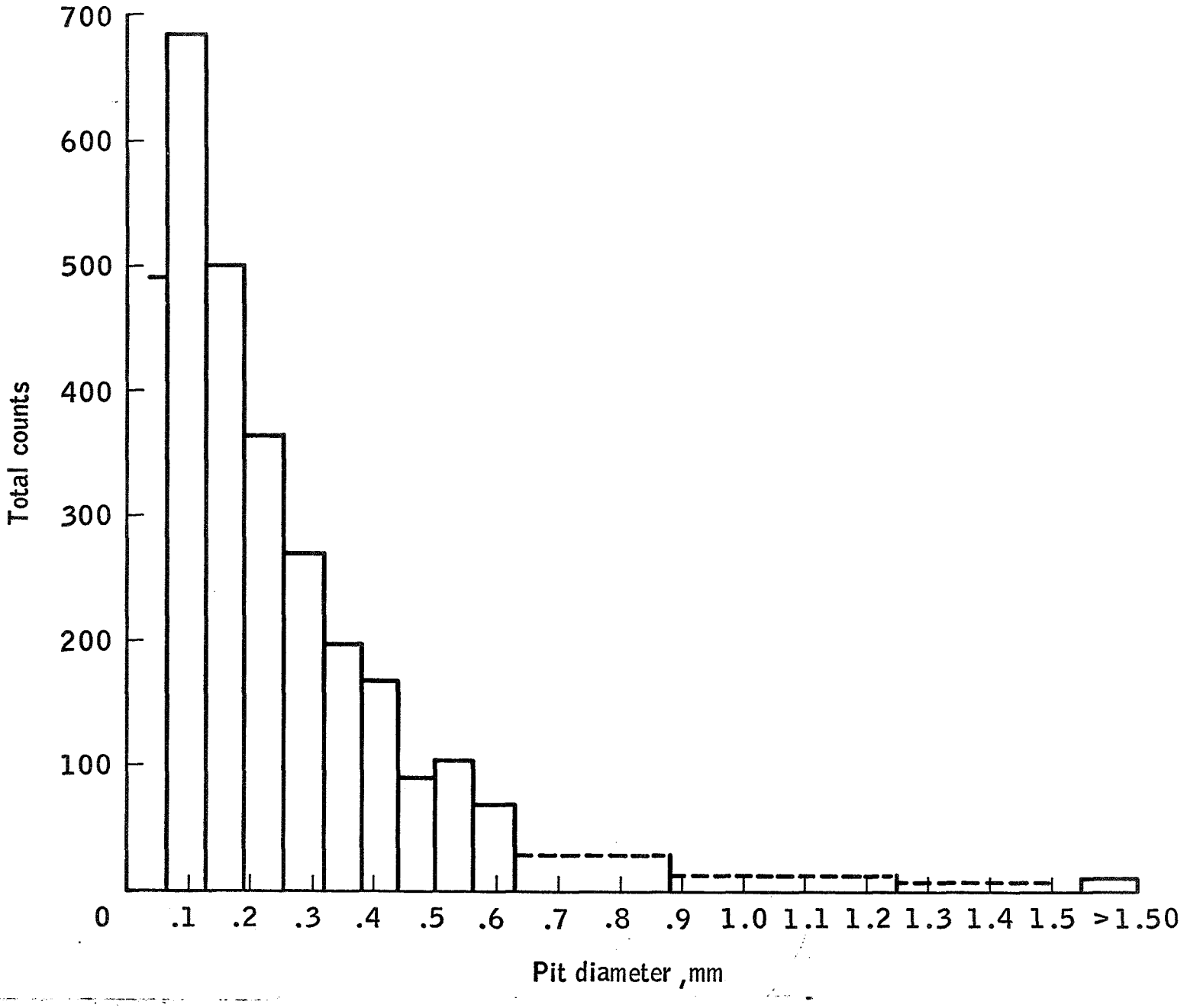
700
600
500
400
300
200
100
0
Total counts
.1
.2
.3
.4
.5
.6
.7
.8
.9
1.0
1.1
1.2
1.3
1.4
1.5
>1.50
Pit diameter, mm

Figure 10

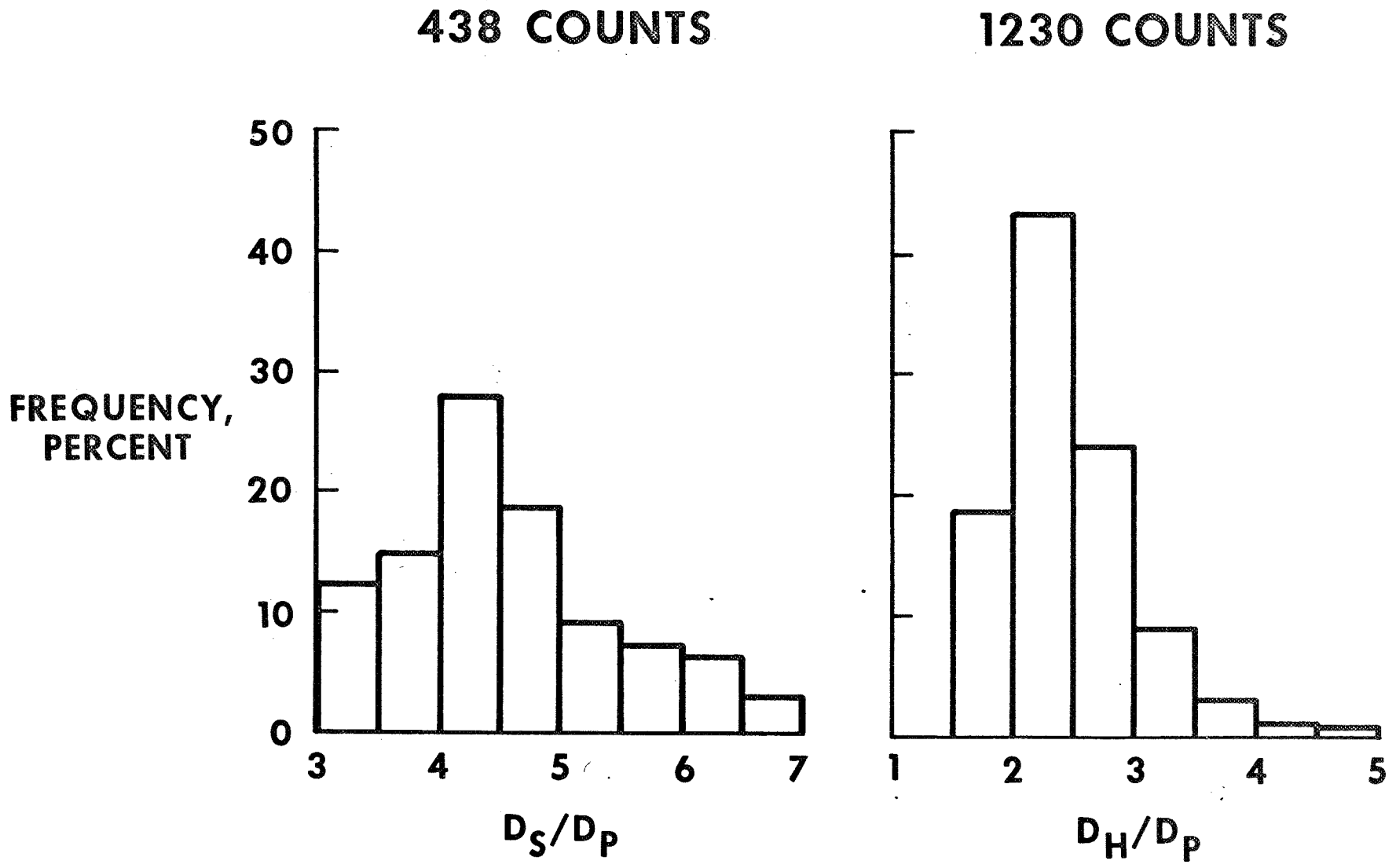
438 COUNTS
1230 COUNTS
FREQUENCY, PERCENT
50
40
30
20
10
0
3
4
5
6
7
1
2
3
4
5
D_S/D_P
D_H/D_P

Figure 11

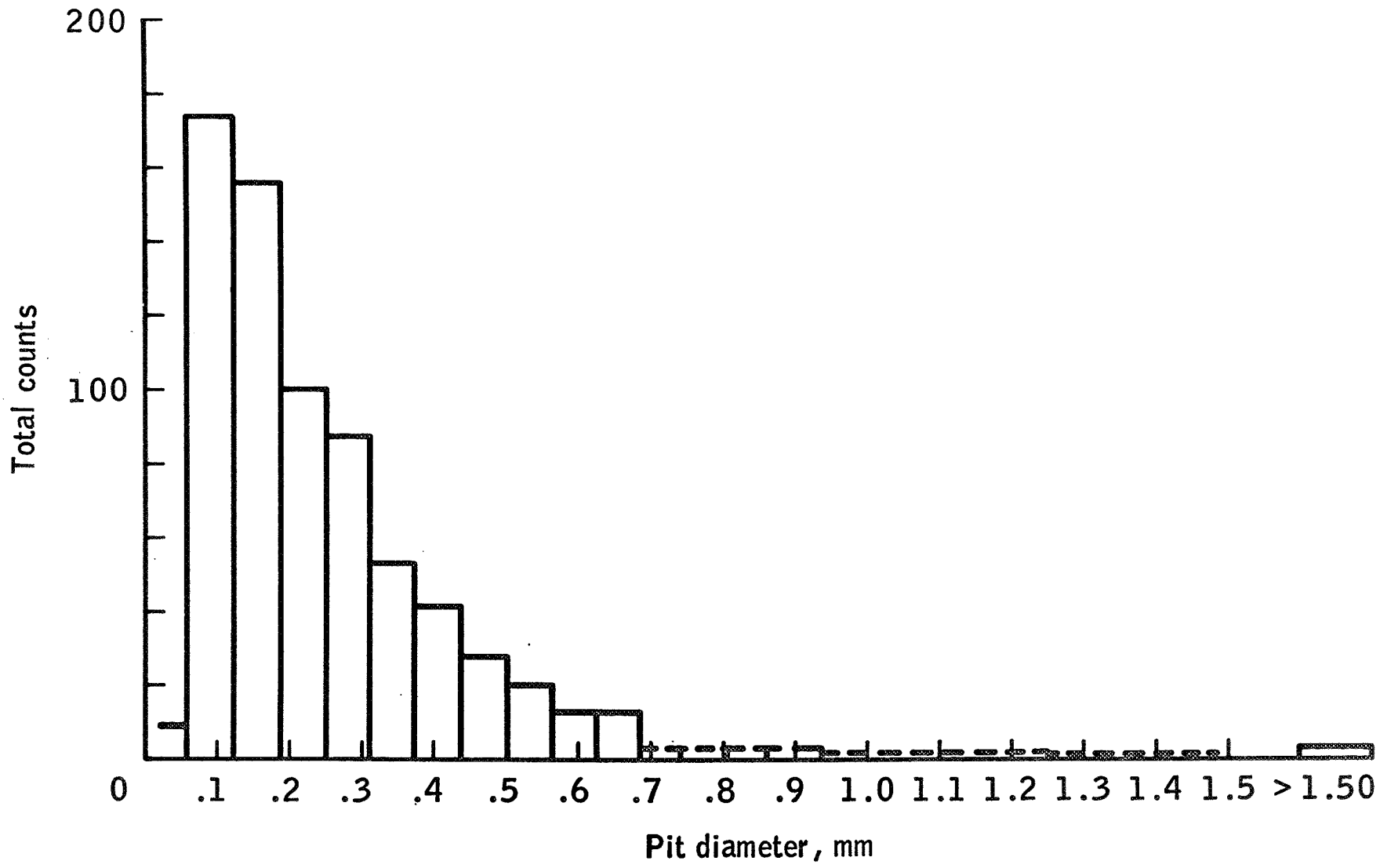
200
100
0
Total counts
.1
.2
.3
.4
.5
.6
.7
.8
.9
1.0
1.1
1.2
1.3
1.4
1.5
>1.50
Pit diameter, mm

Figure 12

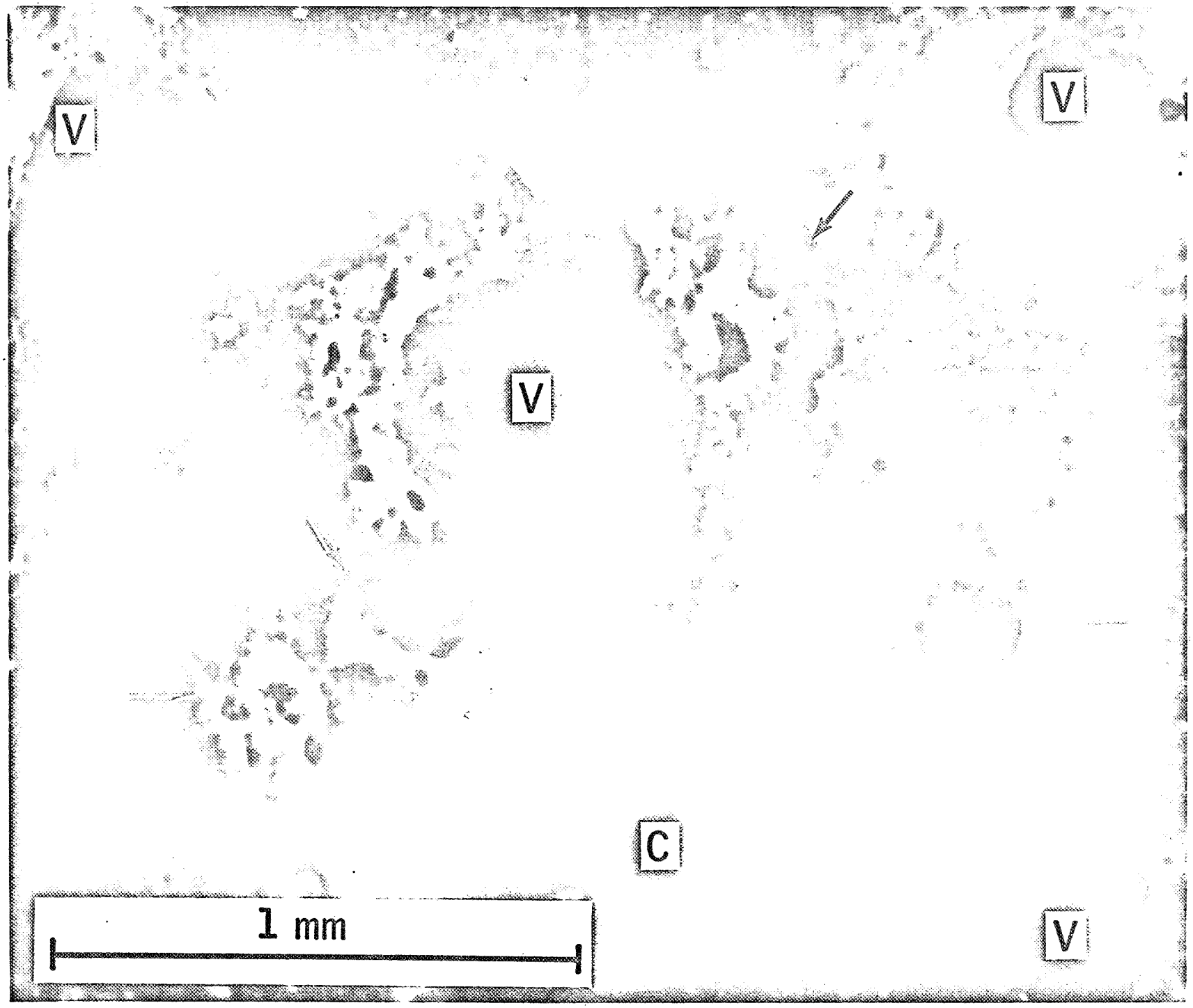

Figure 13

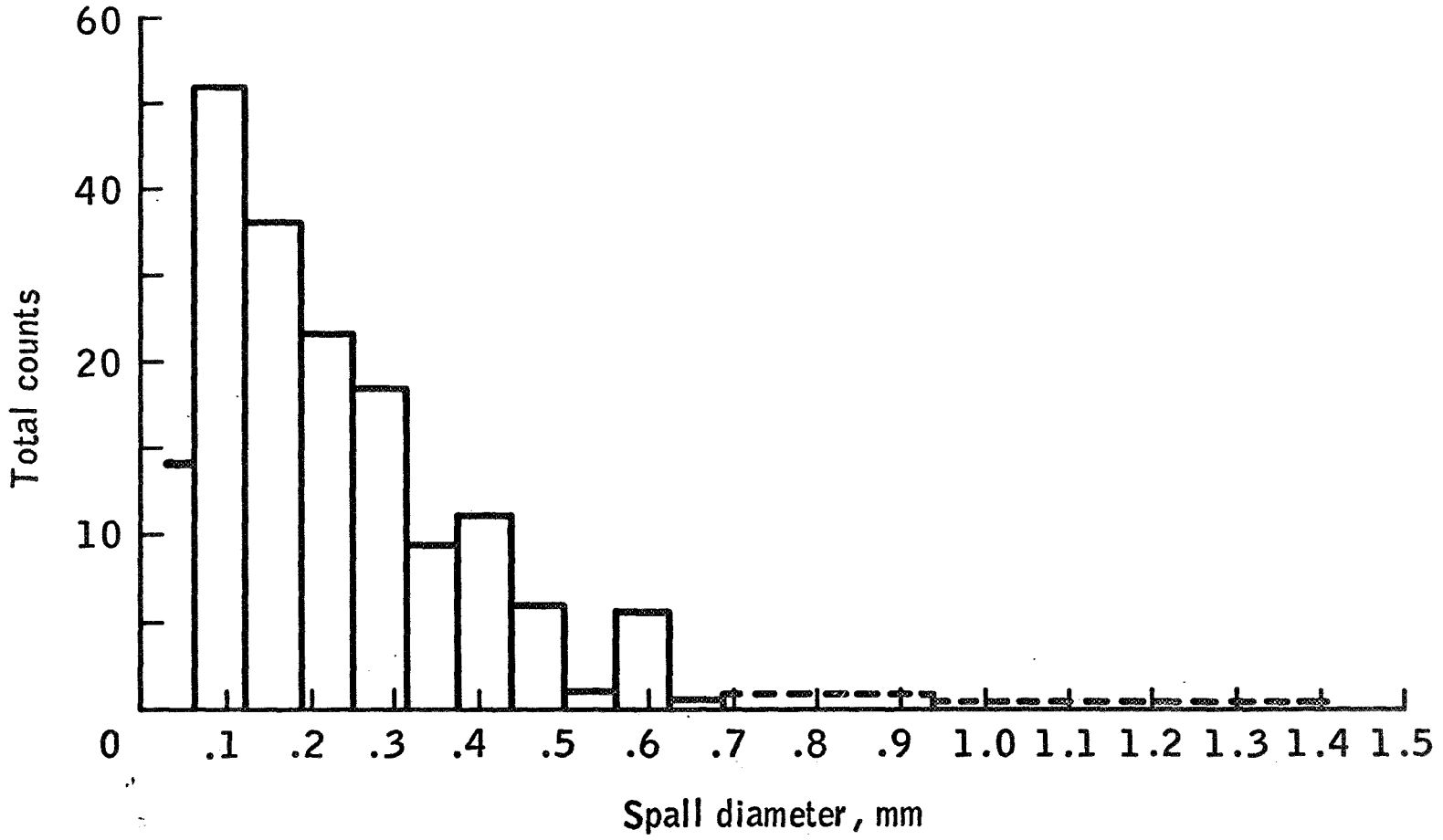
60
40
20
10
0
Total counts
.1
.2
.3
.4
.5
.6
.7
.8
.9
1.0
1.1
1.2
1.3
1.4
1.5
Spall diameter, mm

Figure 14

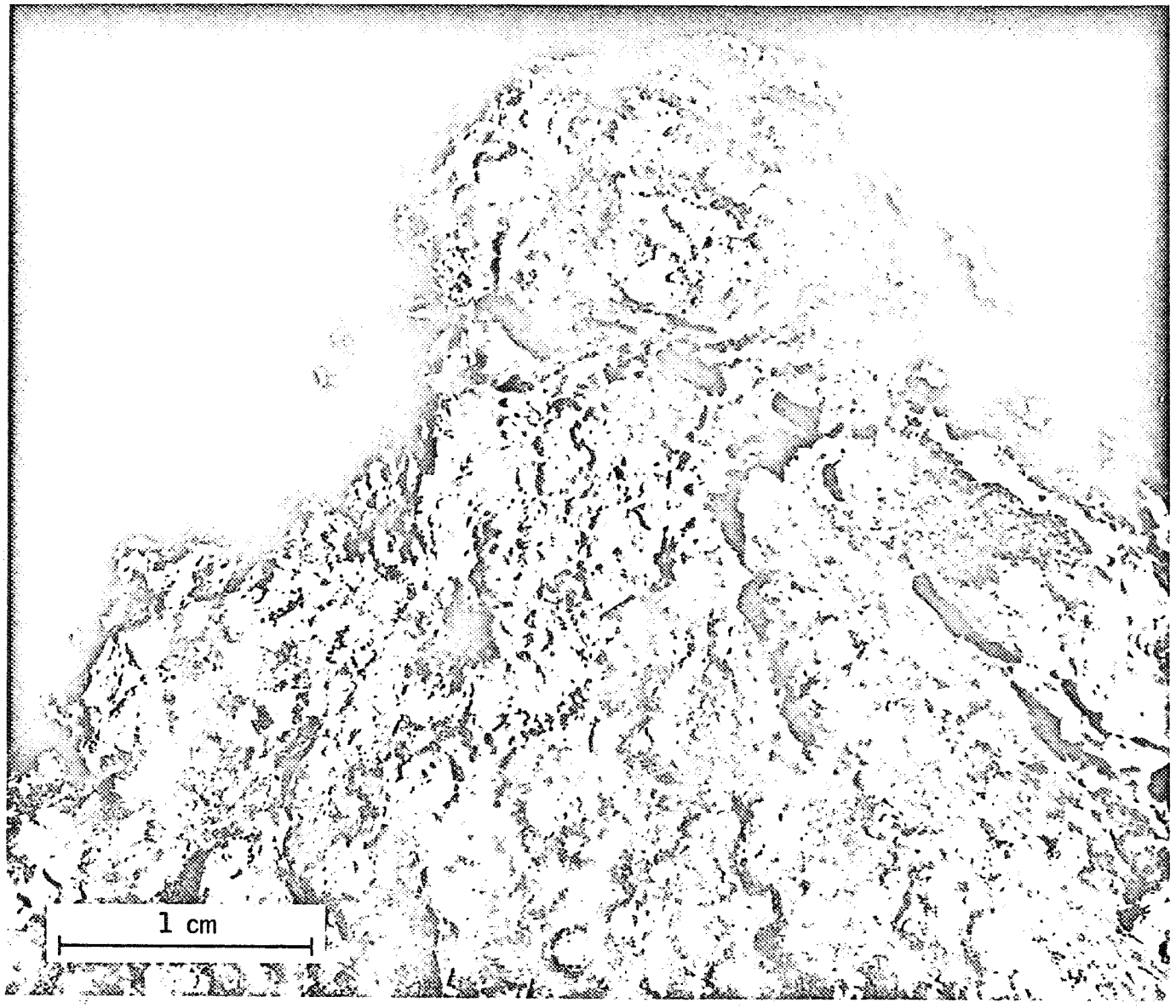

Figure 15

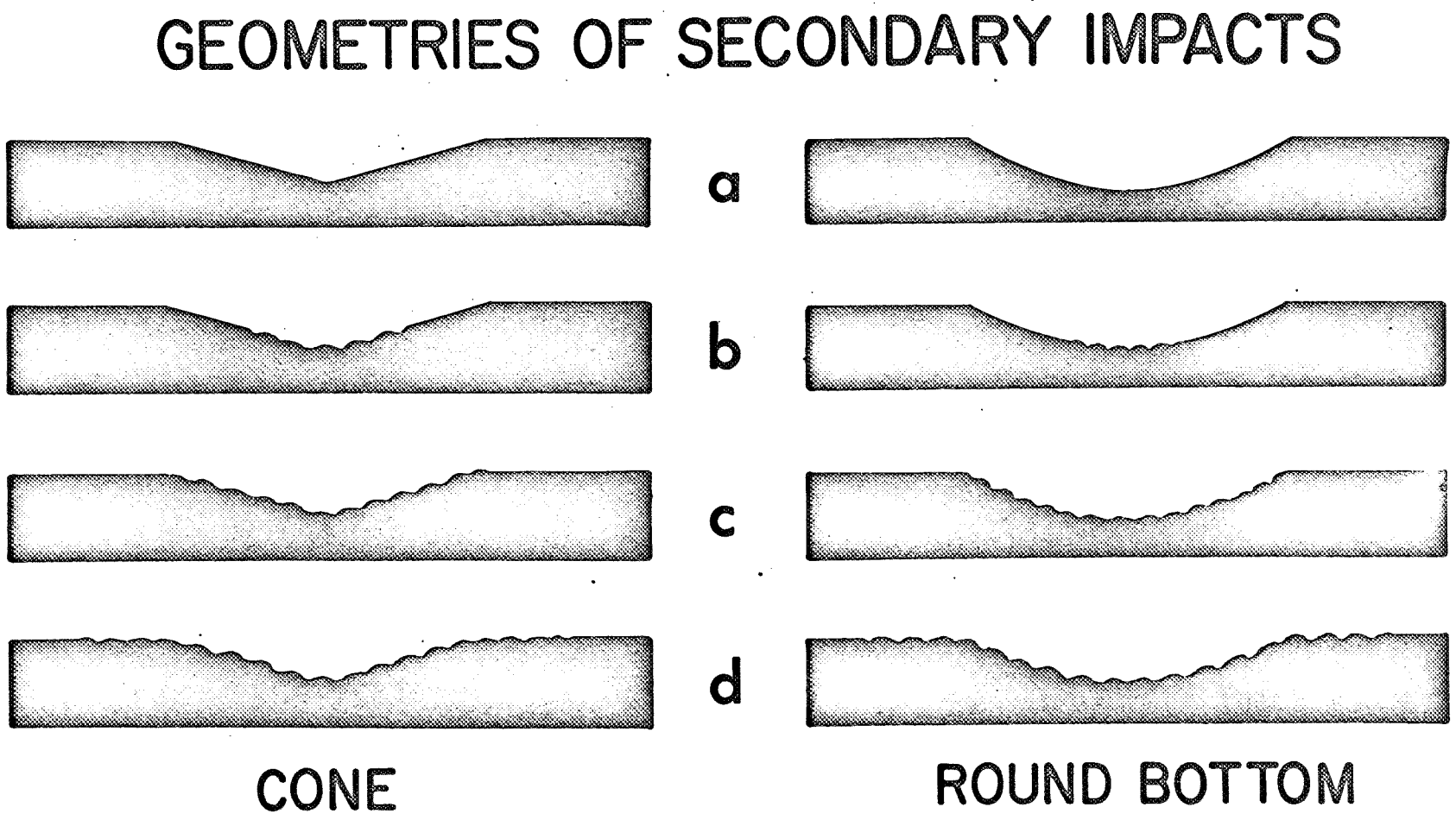

Figure 16

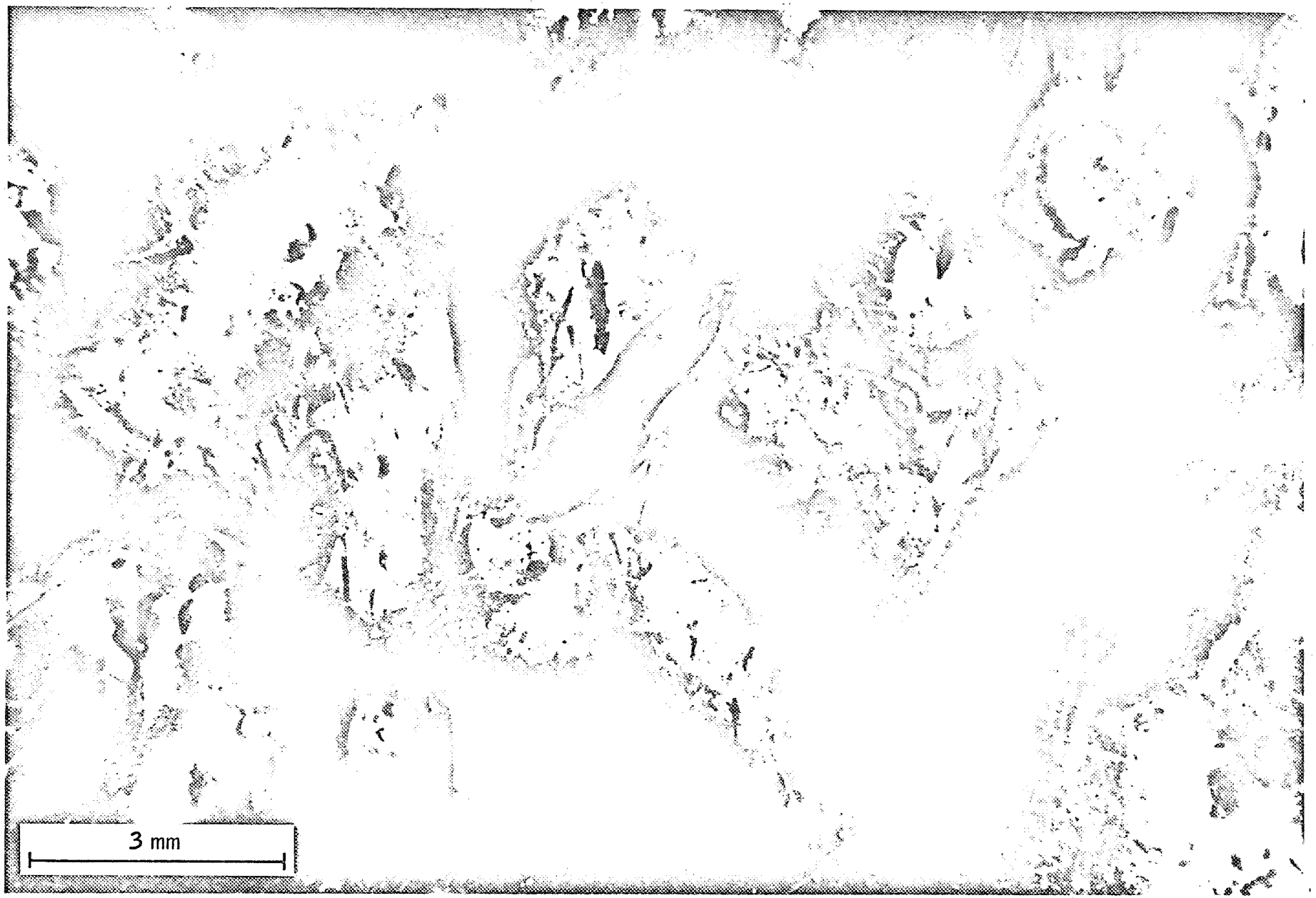

Figure 17

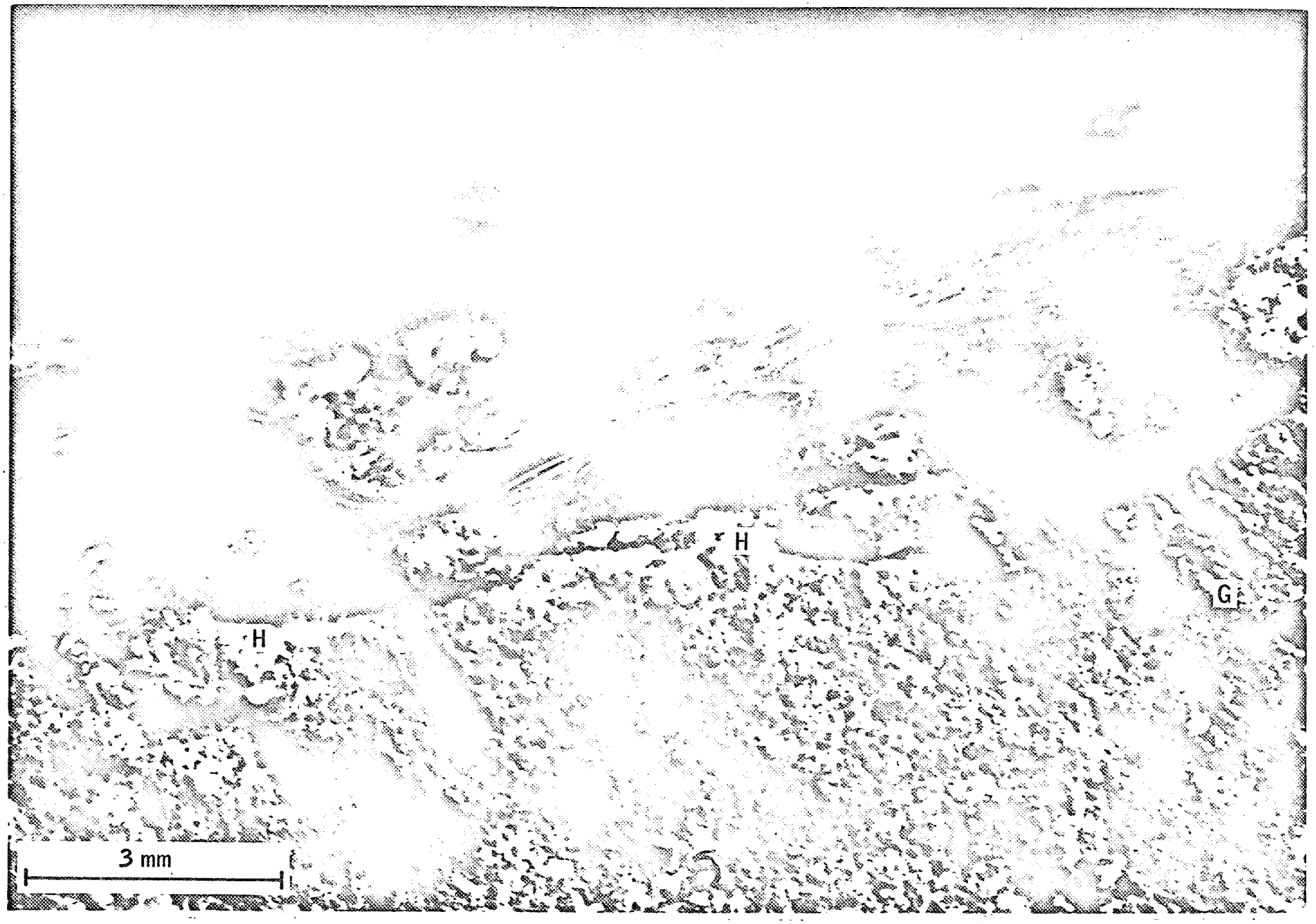

Figure 18

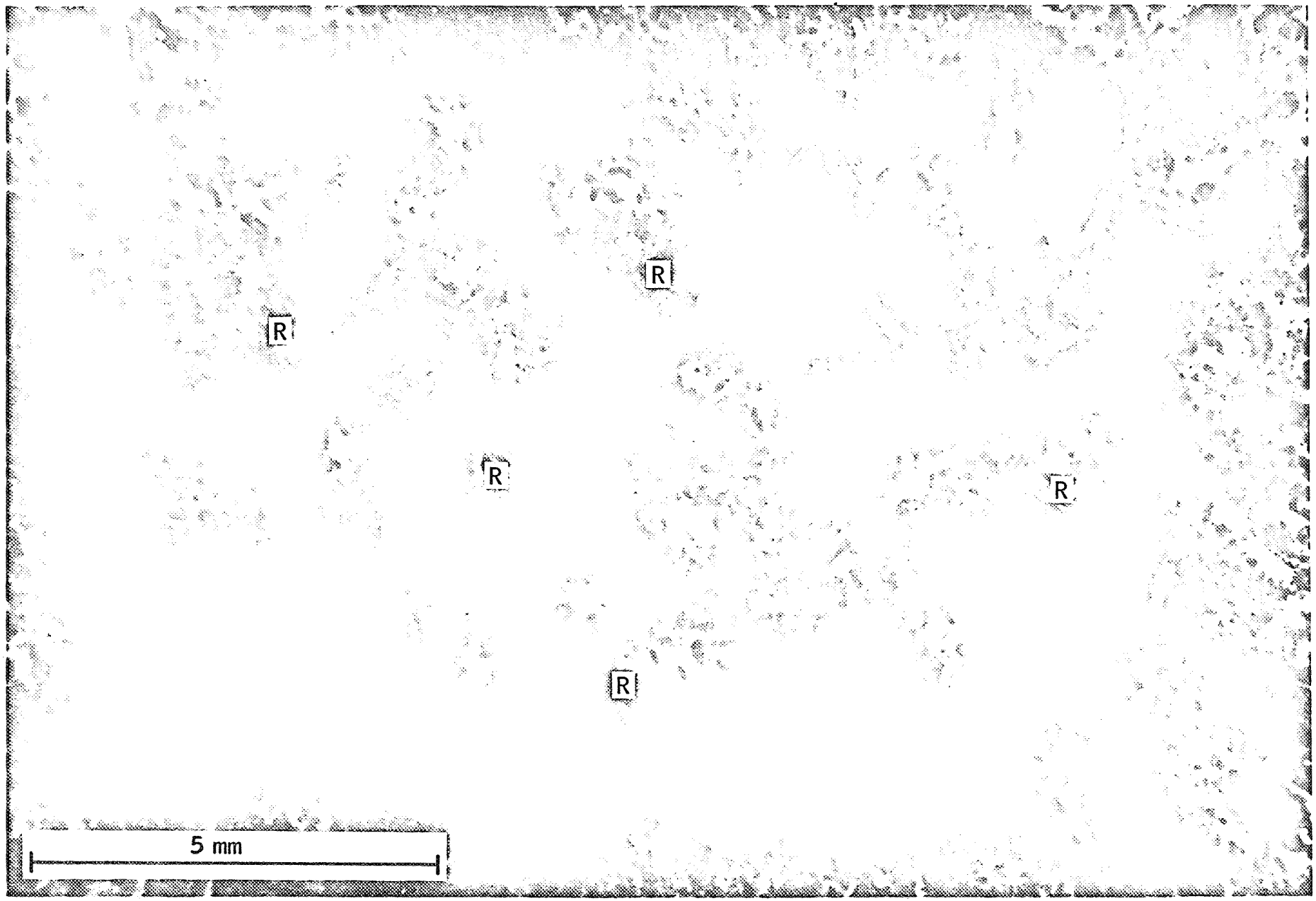

Figure 19

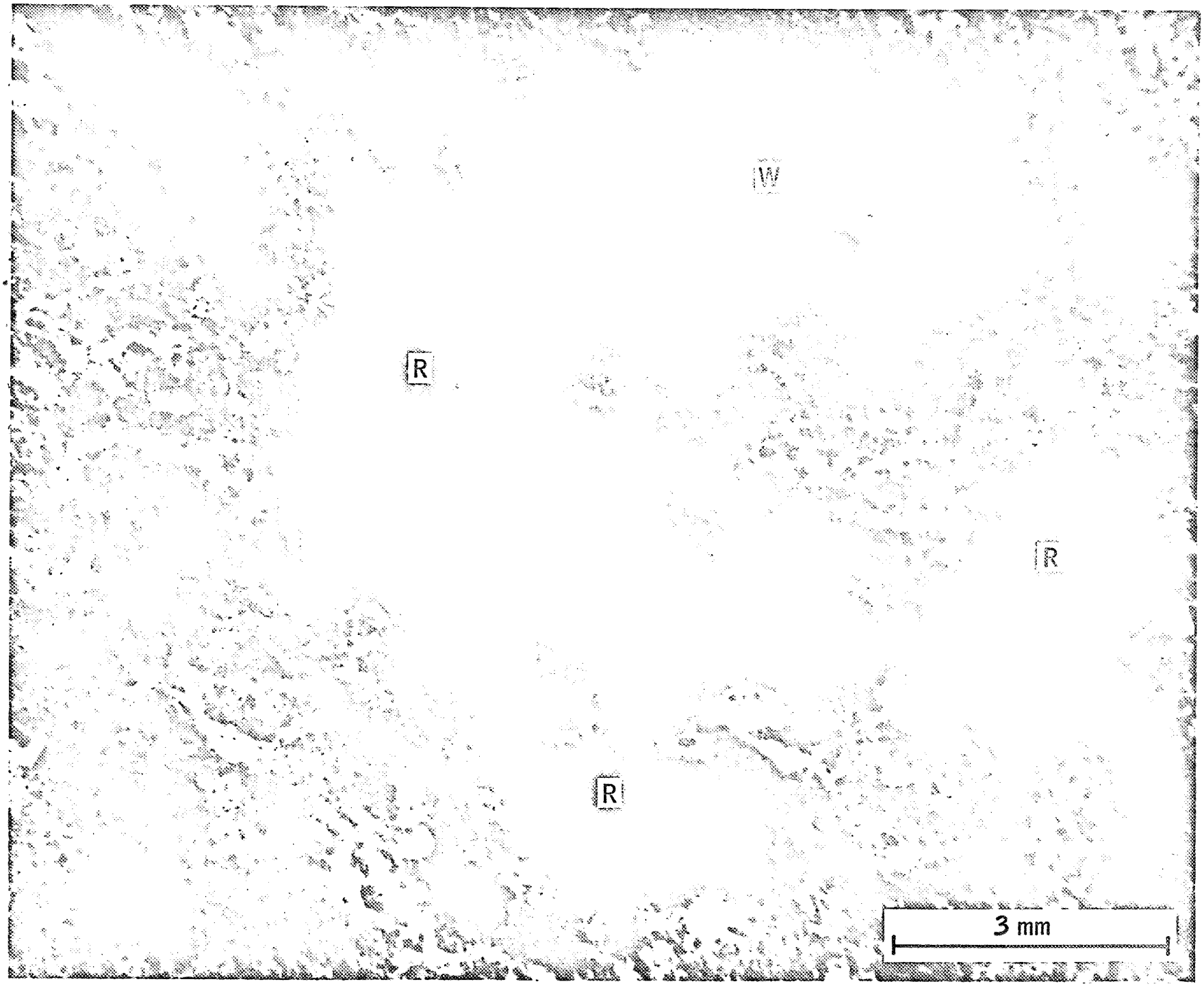

Figure 20

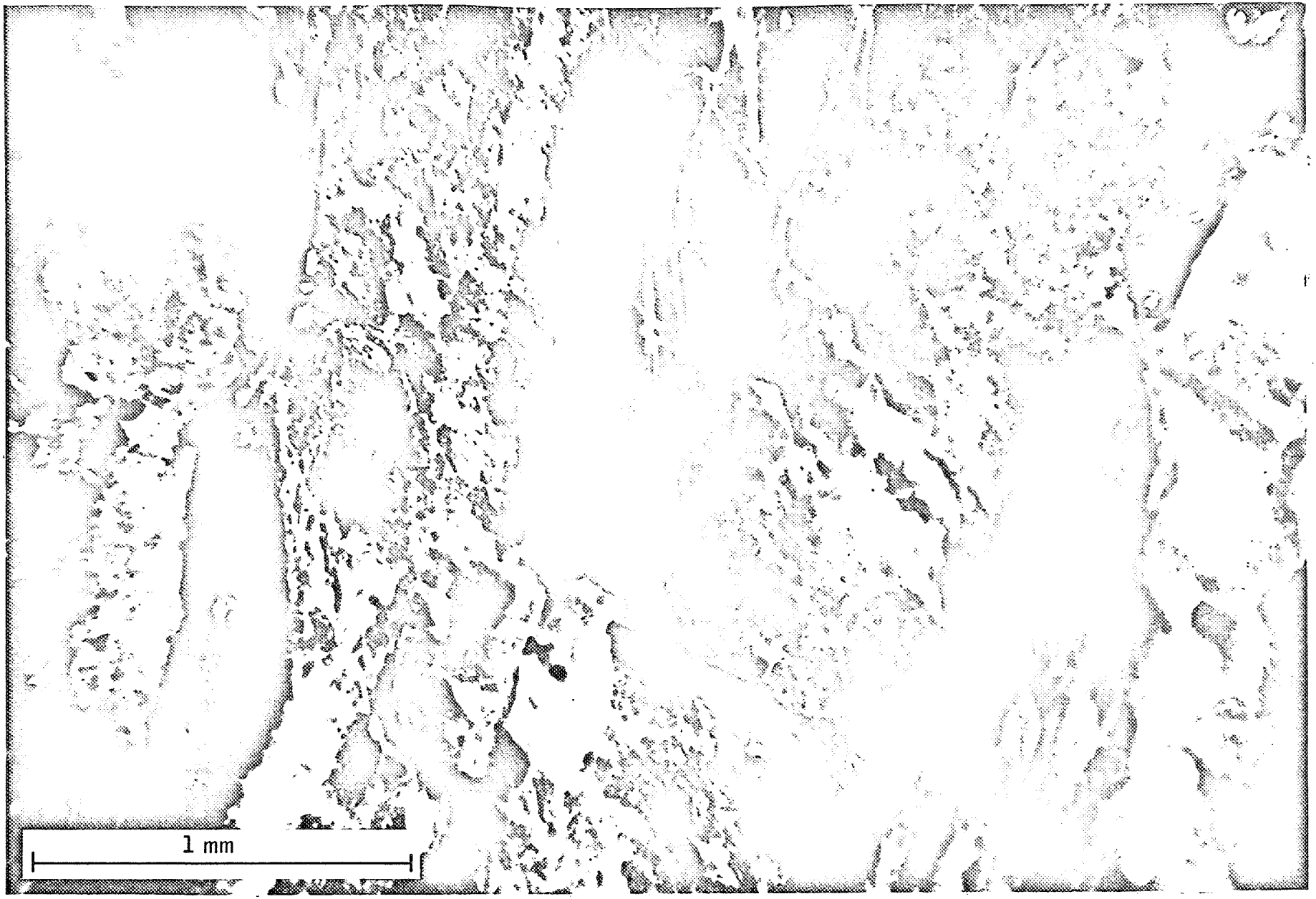

Figure 21

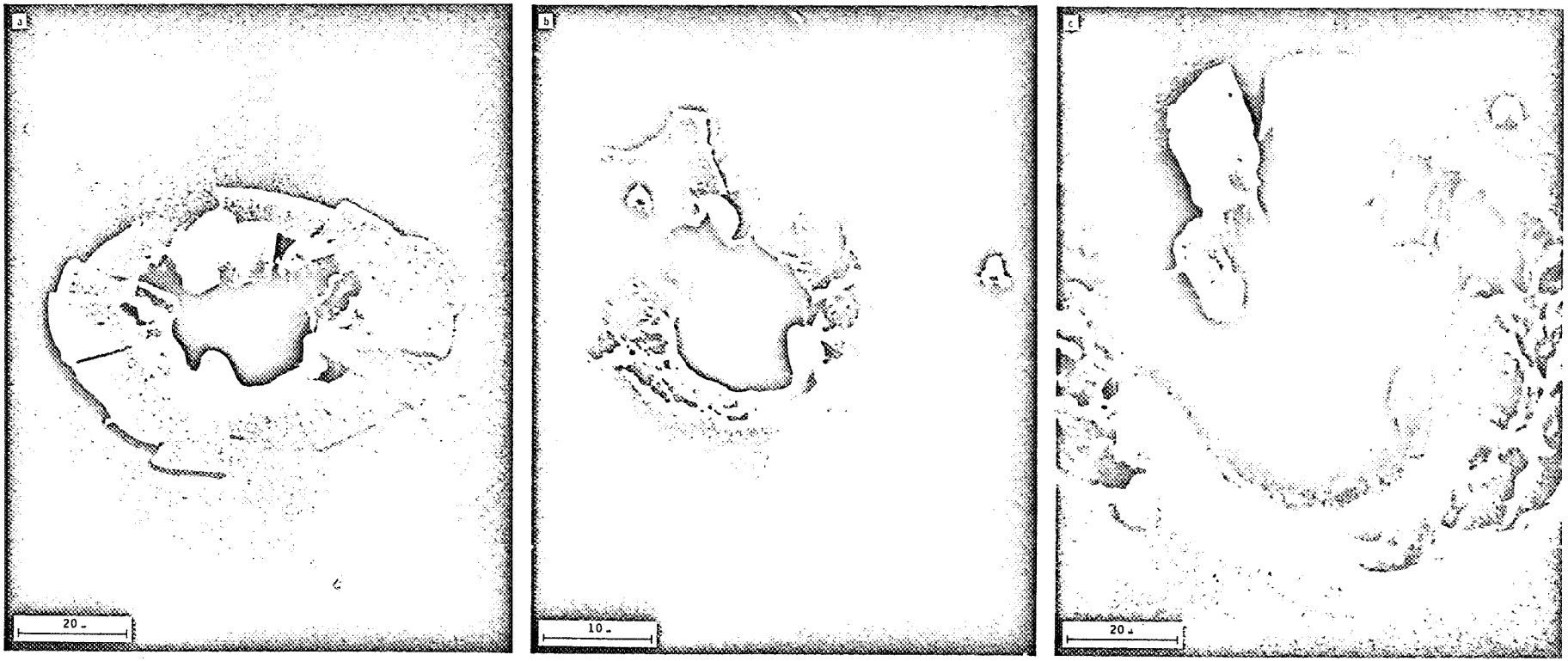

Figure 22

Figure 23

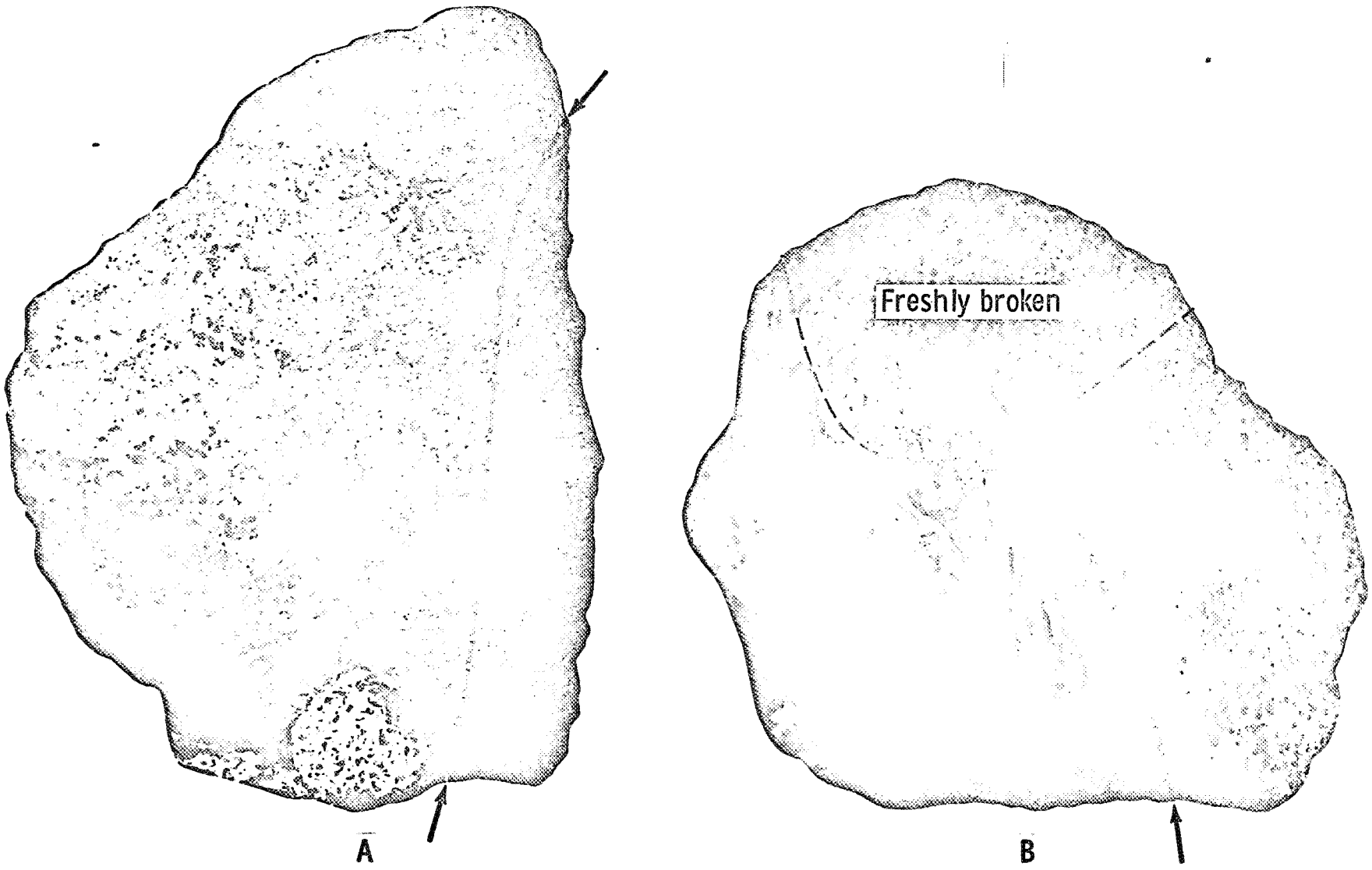

Figure 24

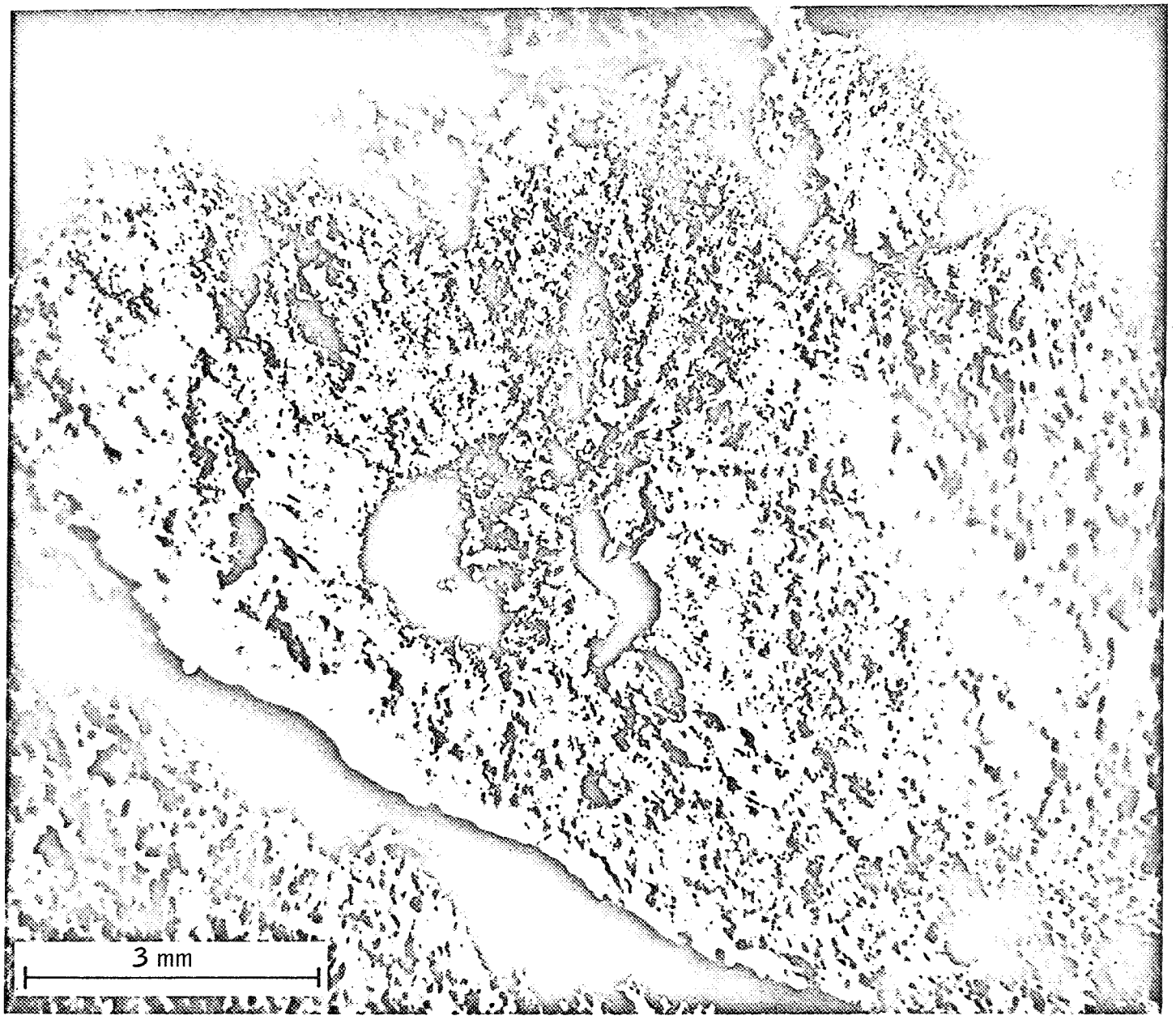

Figure 25

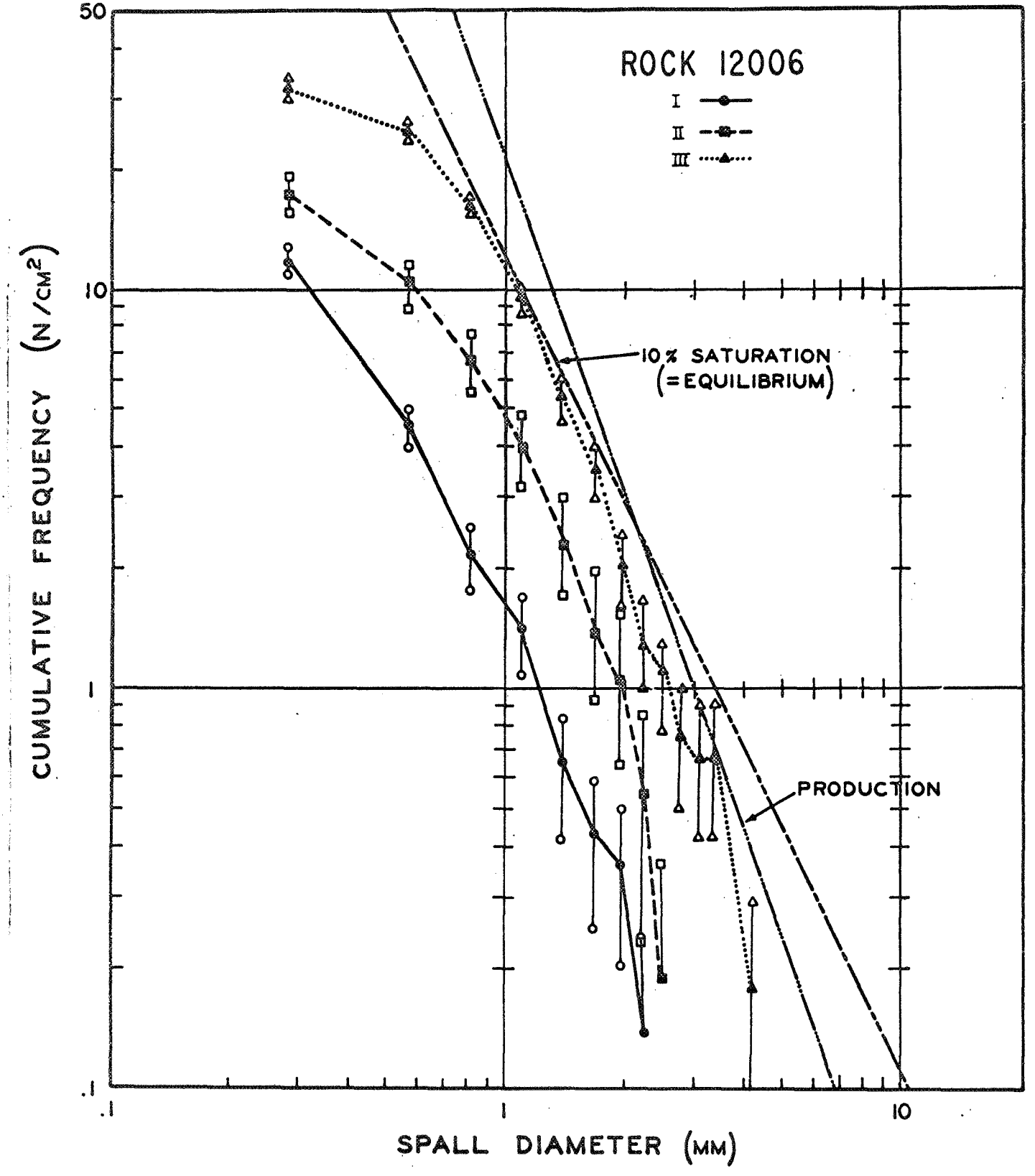
ROCK 12006
I
II
III
10% SATURATION
(=EQUILIBRIUM)
PRODUCTION
CUMULATIVE FREQUENCY (N/CM²)
SPALL DIAMETER (MM)
50
10
1
.1
.1
1
10

Figure 26

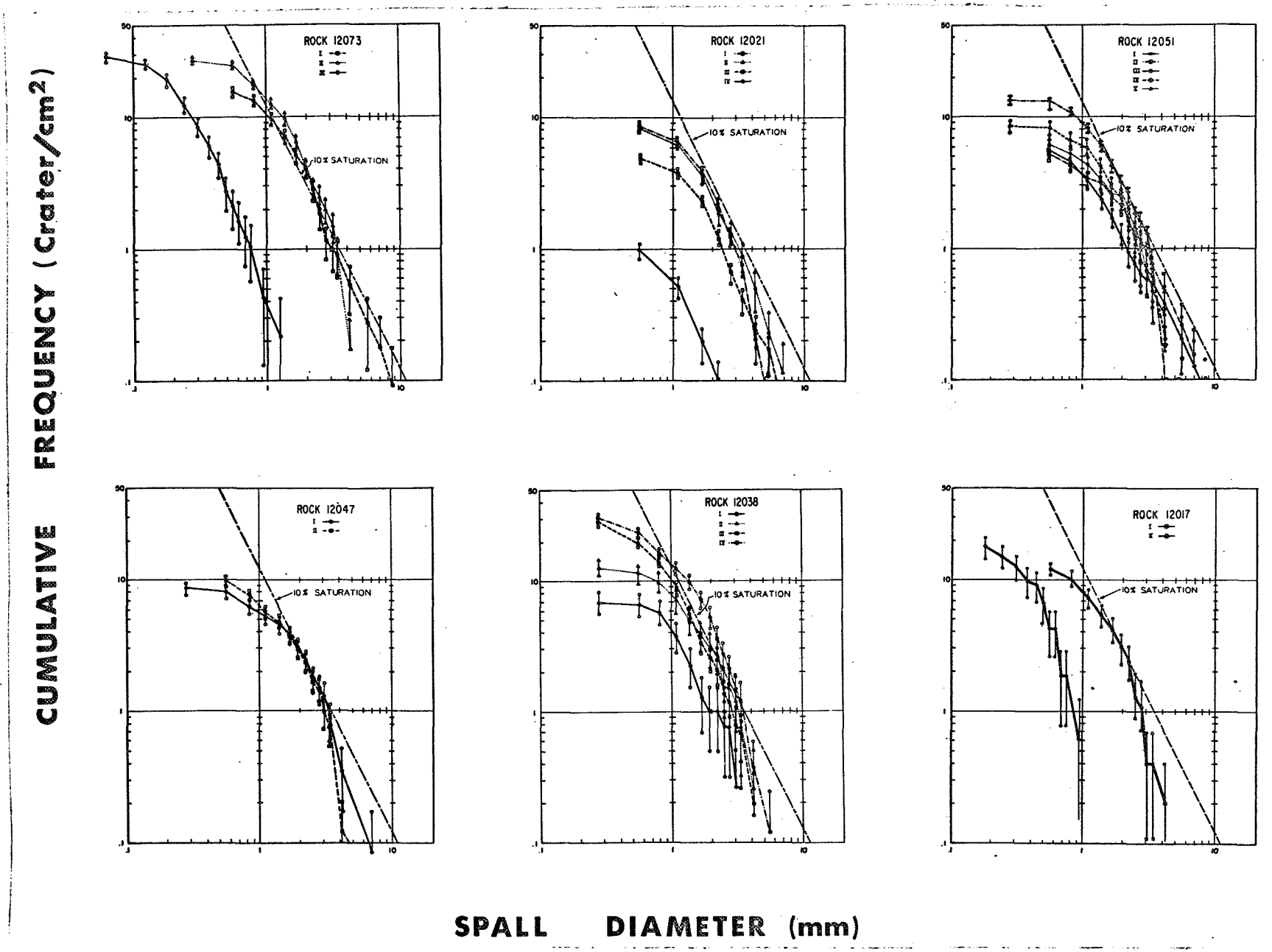
CUMULATIVE FREQUENCY (Crater/cm²)
ROCK 12073
10% SATURATION
ROCK 12021
10% SATURATION
ROCK 12051
10% SATURATION
ROCK 12047
10% SATURATION
ROCK 12038
10% SATURATION
ROCK 12017
10% SATURATION
SPALL DIAMETER (mm)

Figure 27

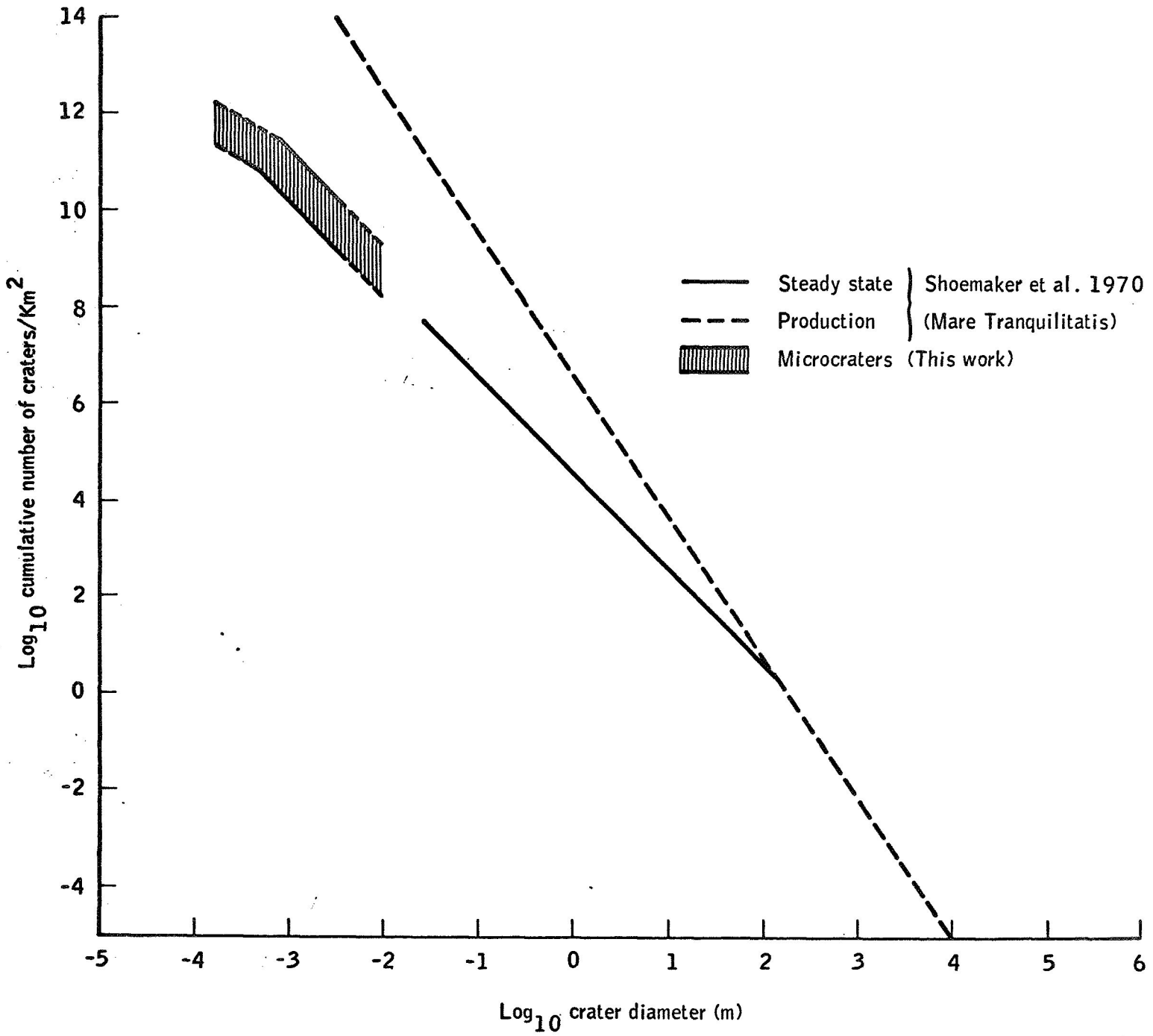
14
12
10
8
6
4
2
0
-2
-4
-5
-4
-3
-2
-1
0
1
2
3
4
5
6
Log10 cumulative number of craters/Km2
Log10 crater diameter (m)
Steady state
Production
Shoemaker et al. 1970
(Mare Tranquilitatis)
Microcraters (This work)

Figure 28

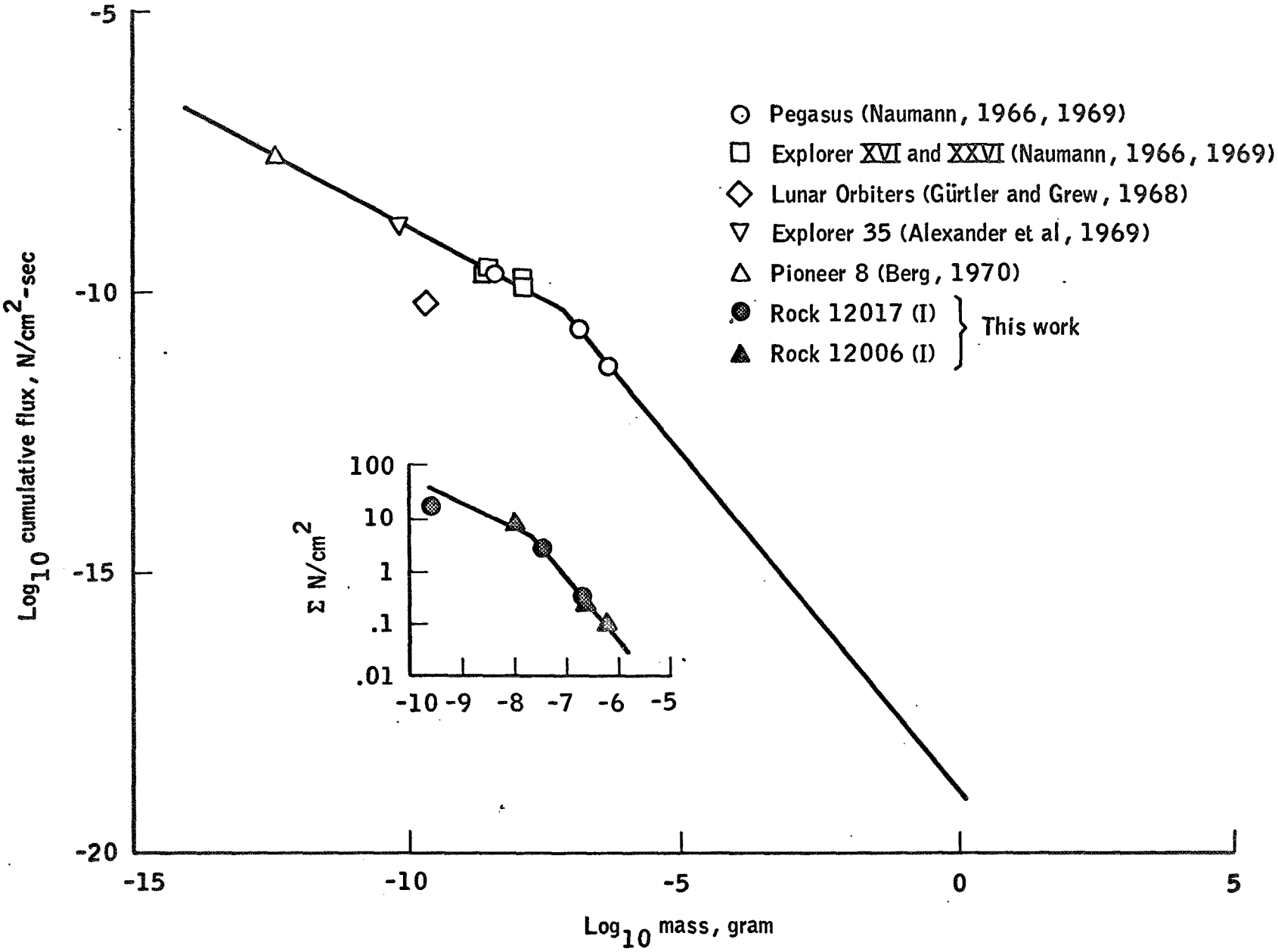
-5
-10
-15
-20
-15
-10
-5
0
5
Log10 cumulative flux, N/cm2-sec
Log10 mass, gram
Pegasus (Naumann, 1966, 1969)
Explorer XVI and XXVI (Naumann, 1966, 1969)
Lunar Orbiters (Gürtler and Grew, 1968)
Explorer 35 (Alexander et al, 1969)
Pioneer 8 (Berg, 1970)
Rock 12017 (I)
Rock 12006 (I)
This work
Σ N/cm2
100
10
1
.1
.01
-10 -9 -8 -7 -6 -5

Figure 29

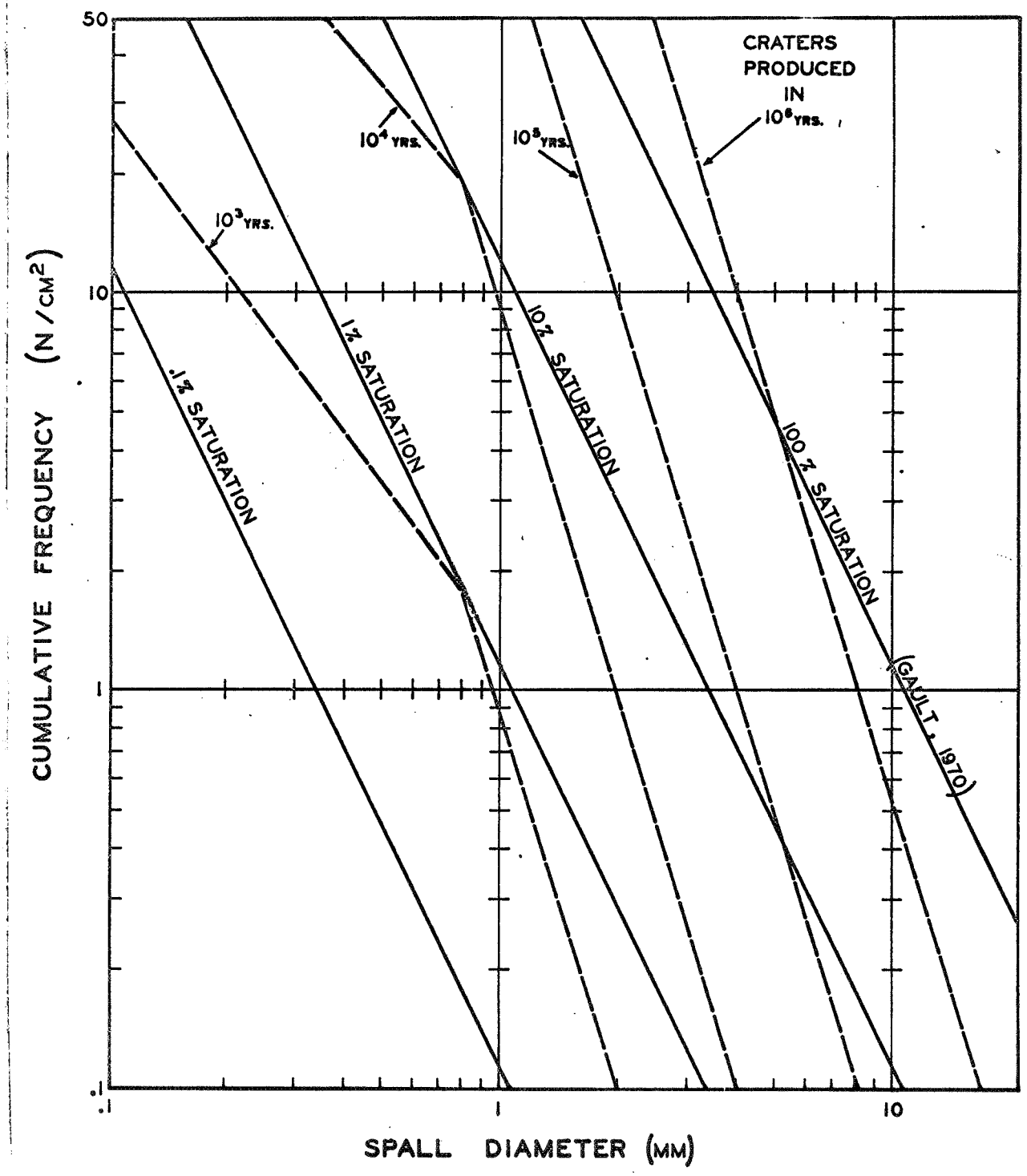

Figure 30